Homoclinic saddle-node bifurcations in singularly perturbed systems

Arjen Doelman and Geertje Hek

Mathematisch Instituut
Universiteit Utrecht
P.O.Box 80.010
3508 TA Utrecht
the Netherlands

October 23, 1997

Abstract

In this paper we study the creation of homoclinic orbits by saddle-node bifurcations. Inspired on similar phenomena appearing in the analysis of so-called 'localized structures' in modulation or amplitude equations, we consider a family of nearly integrable, singularly perturbed three dimensional vector fields with two bifurcation parameters a and b.

The $O(\varepsilon)$ perturbation destroys a manifold consisting of a family of integrable homoclinic orbits: it breaks open into two manifolds, $W^{\rm s}(\Gamma)$ and $W^{\rm u}(\Gamma)$, the stable and unstable manifolds of a slow manifold Γ. Homoclinic orbits to Γ correspond to intersections $W^{\rm s}(\Gamma) \cap W^{\rm u}(\Gamma)$; $W^{\rm s}(\Gamma) \cap W^{\rm u}(\Gamma) = \emptyset$ for $a < a^*$, a pair of 1-*pulse* homoclinic orbits emerges as *first* intersection of $W^{\rm s}(\Gamma)$ and $W^{\rm u}(\Gamma)$ as $a > a^*$. The bifurcation at $a = a^*$ is followed by a sequence of nearby, $O(\varepsilon^2(\log \varepsilon)^2)$, homoclinic saddle-node bifurcations at which pairs of N-pulse homoclinic orbits are created (these orbits make N circuits through the fast field).

The second parameter b distinguishes between two significantly different cases: in the *cooperating* (respectively *counteracting*) case the averaged effect of the fast field is in the same (respectively opposite) direction as the slow flow on Γ. The structure of $W^{\rm s}(\Gamma) \cap W^{\rm u}(\Gamma)$ becomes highly complicated in the counteracting case: we show the existence of many new types of sometimes exponentially close homoclinic saddle-node bifurcations.

The analysis in this paper is mainly of a geometrical nature.

1 Introduction

In this paper we study a three-dimensional nearly integrable system of ordinary differential equations with two bifurcation parameters a and b:

$$\left\{ \begin{array}{rcl} \dot{x} &=& y \\ \dot{y} &=& x - x^2 + \varepsilon y(z^2 - a) \\ \dot{z} &=& \varepsilon(1 + bx). \end{array} \right. \tag{1.1}$$

where $0 < \varepsilon \ll 1$. In the integrable limit $\varepsilon \to 0$, the system contains two manifolds of degenerate equilibria, $\{x = y = 0\}$ and $\{x = 1, y = 0\}$ and a two-dimensional homoclinic manifold $\mathcal{H}$ that limits on the line of degenerate saddles

$$\Gamma = \{x = y = 0\} \tag{1.2}$$

(see Figure 1). Nearly integrable three-dimensional systems similar to this model problem appear in a natural fashion in the analysis of (generalized) modulation or amplitude equations of the type:

$$\frac{\partial A}{\partial t} = \alpha \frac{\partial^2 A}{\partial x^2} + f_1(|A|^2)A + i\frac{\partial}{\partial x}[f_2(|A|^2)A] + iA\frac{\partial}{\partial x}[f_3(|A|^2)] \tag{1.3}$$

where $A(x,t) : \mathbf{R} \times \mathbf{R}^+ \to \mathbf{C}$ and $\alpha \in \mathbf{C}$; $f_i(|A|^2)$, $i = 1,2,3$ are complex valued real analytic functions ([20]). These equations can be derived by a weakly nonlinear analysis near the onset of instability ([20], [7]). The (cubic) Ginzburg-Landau equation and the nonlinear Schrödinger equation are included in (1.3) by choosing $f_1(|A|^2) = \beta + \gamma|A|^2$ and $f_{2,3} \equiv 0$, where $\beta, \gamma \in \mathbf{C}$ for the Ginzburg-Landau case and $\beta = 0$, $\alpha, \gamma \in i\mathbf{R}$ for the nonlinear Schrödinger case. However, f_1 can certainly also be a quintic polynomial (see for instance [14], [2],[16]) and f_2 and f_3 are not necessarily trivial (see for instance [3], [6]). We refer to [20] and the references given there for more background on equations of the type (1.3). Traveling, time-periodic solutions of the form $A(x,t) = A(x - ct)e^{iwt}$ are described by the ODE reduction

$$\alpha A'' + cA' - iwA + f_1(|A|^2)A + i[f_2(|A|^2)A]' + iA[f_3(|A|^2)]' = 0 \tag{1.4}$$

where $' = d/d\xi$ with $\xi = x - ct$. Systems like (1.4) have been extensively studied in the literature, see [10], [3], [14], [20], [6], [2], [16] and the references given there. By introducing polar coordinates, $A(\xi) = \rho(\xi)e^{i\theta(\xi)}$, (1.4) reduces to a *three*-dimensional (real) system in (ρ, ρ', θ') ((1.4) is invariant with respect to the phase shift $A \to Ae^{i\psi}$). It is easy to check that there are (at least) two special cases in which this system is integrable: $\alpha \in \mathbf{R}$, $c = w = 0$ and f_i real valued ($i = 1,2,3$) or $\alpha \in i\mathbf{R}$ and $f_i(|A|^2) \in i\mathbf{R}$ ($i = 1,2,3$) (see [3], [20]). Note that the real Ginzburg-Landau equation is of the first type, and that the nonlinear Schrödinger equation is of the second type ([20], [2]). In general, these special integrable cases also relate to systems of considerable physical relevance. For instance, the first case appears naturally when performing a weakly nonlinear stability analysis in reversible systems ([3], [20]). Small ($O(\varepsilon)$, $0 < \varepsilon \ll 1$) perturbations of such an integrable system result in a nearly integrable system of the following type ([3], [20], [2]):

$$\left\{ \begin{array}{lcl} \rho' & = & V \\ V' & = & F(\rho, \Omega) + \varepsilon g_1(\rho, V, \Omega; \varepsilon) \\ \Omega' & = & \varepsilon g_2(\rho, V, \Omega; \varepsilon) \end{array} \right. \tag{1.5}$$

The perturbed Schrödinger equation ([16], [20]) is another example of an equation covered by (1.5).

System (1.1) is a highly simplified model problem of the type (1.5). We refer to [5] for a 'phenomenological' derivation of a system similar to (1.1) – and with the same integrable limit – based on certain essential properties of (1.5) in the case of the cubic

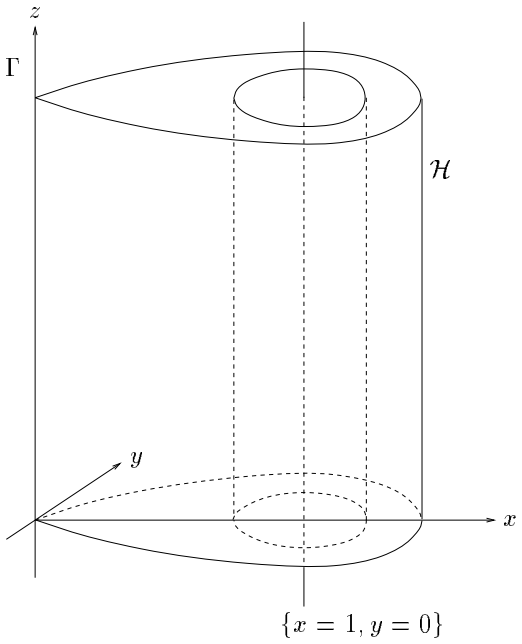

Figure 1: The phase portrait of the unperturbed system.

Ginzburg-Landau equation. In this paper we study (1.1) to obtain a both qualitative – or geometrical – and a quantitative understanding of a certain type of co-dimension 1 homoclinic saddle-node bifurcation that appears in singularly perturbed systems of the type (1.5). As in [5], the main reason to study a model problem instead of a system derived from (1.3), is that the simplicity of (1.1) enables us to focus on the essential mechanisms involved in these global saddle-node bifurcations: model (1.1) has been constructed to only describe one of the numerous (global) phenomena that appear in systems as (1.5) (see Remark 1.1). Likewise, the model problem studied in [5] was derived to analyse the interactions of local saddle-node bifurcations and global recurrent orbits. Both phenomena occur in the Ginzburg-Landau equation ([2]). Moreover, basic calculations, such as the computation of the equivalent of the normally hyperbolic manifold Γ (1.2), the analysis of local bifurcations, etc., are quite cumbersome in explicit systems of the type (1.5) – see for instance [2]. Furthermore, in these systems many degenerations, such as the singularity near $\rho = 0$ and the fact that Γ is not always normally hyperbolic, occur. These degenerations are not at all relevant to the analysis, but it takes quite a technical effort to control them. Therefore, the analysis of model problem (1.1) can be seen as a first step in understanding more complex systems of the type (1.5). Since the methods developed in this paper are mostly of a geometrical nature, the problems when taking the next step will have a computational, but not a conceptual, character.

In order to describe the homoclinic saddle-node bifurcation to be studied in this paper, we first need to appeal to some fundamental results due to Fenichel ([8], [12]). Since Γ (1.2) is normally hyperbolic in the limit $\varepsilon \to 0$, both Γ and its (two-dimensional) stable and unstable manifolds, $W^{\mathrm{s}}(\Gamma)$ and $W^{\mathrm{u}}(\Gamma)$, persist under the perturbation (see section 2 for more details: we do not need to distinguish between Γ_0 (i.e. $\varepsilon = 0$) and Γ_ε here; in

general Γ_0 and Γ_ε are $O(\varepsilon)$ apart). However, $W^{\rm s}(\Gamma)$ and $W^{\rm u}(\Gamma)$ merge on the homoclinic manifold $\mathcal{H}$ when $\varepsilon = 0$ (Figure 1), while in general they will only intersect in a (discrete) number of one-dimensional curves when $\varepsilon \neq 0$ (see Figure 2). These curves are solutions to (1.1) that are biasymptotic to Γ; Γ is called the slow manifold for $\varepsilon \neq 0$. Such homoclinic solutions are extremely important in the context of (1.5) and the modulation equations (1.3): they represent so-called traveling, localized or coherent 'structures', such as fronts and domain walls ([10], [3], [14], [20], [6], [2], [16]).

The model problem (1.1) is constructed such that $W^{\rm s}(\Gamma) \cap W^{\rm u}(\Gamma) = \emptyset$ for $a < a^* = O(\varepsilon)$ – see section 2. At $a = a^*$, $W^{\rm s}(\Gamma)$ and $W^{\rm u}(\Gamma)$ intersect non-transversally: there is a unique homoclinic orbit $\gamma_{\rm int}(t)$ that splits into two homoclinic orbits $\gamma_{\rm int}^+(t)$ and $\gamma_{\rm int}^-(t)$ when $a > a^*$ (Theorem 4.7, Figure 3). We call these orbits 1-pulse homoclinic orbits since they make one circuit through the 'fast' field, following a (planar) homoclinic orbit of the unperturbed system. We show that this first homoclinic saddle-node bifurcation is 'quickly' followed by a second saddle-node bifurcation at $a = a_2^* = a^* + O(\varepsilon^2(\log\varepsilon)^2)$ at which two 2-pulse homoclinic orbits are created (Theorems 4.7 and 5.1, Figure 4): these orbits make two circuits through the fast field. Two 3-pulse homoclinic orbits are created at the next bifurcation at $a = a_3^* = a_2^* + O(\varepsilon^2(\log\varepsilon)^2)$, etc.. This process has created $O(|\log\varepsilon|)$ N-pulse orbits (two for each $N \leq O(|\log\varepsilon|)$) as a has become $O(1)$ and positive (Theorem 4.2).

The above results seem to be completely independent of the second parameter b and in a sense they are: the N-pulse orbits exist for all b when $a = O(1)$ (Theorem 6.1). However, b can have a dramatic influence on the structures of $W^{\rm s}(\Gamma)$ and $W^{\rm u}(\Gamma)$. Therefore, we distinguish in this paper between two cases: the *cooperating* case and the *counteracting* case. In the cooperating case the accumulated growth of z during one circuit through the fast field is in the same (positive) direction as the slow flow along Γ. The way b appears in (1.1) is chosen is such a way, that it controls the sign and magnitude of the z-component of the averaged flow in the fast field. Note that we only need to control a one-dimensional quantity (the z-component): it suffices to introduce a one-dimensional parameter. We show in section 2 that the cooperating case corresponds to the choice $b > -1$ (this includes the case $b = 0$ where z can be interpreted as a slow time variable). In the cooperating case all possible intersections of $W^{\rm s}(\Gamma)$ and $W^{\rm u}(\Gamma)$ are described in the above paragraph (and Figure 3). However, the structure of $W^{\rm s}(\Gamma)$ and $W^{\rm u}(\Gamma)$ becomes much more complicated in the counteracting case when b decreases through -1: the averaged displacement in the z-direction can now become negative. In Theorems 6.3, 6.4 and 6.6 we construct a sequence of *first* homoclinic saddle-node bifurcations,

$$b_{1,2}^i < b_2^{ii} < b_2^i < b_{2,3}^{ii} < b_{2,3}^i < b_3^{ii} < \ldots < b_n^{ii} < b_n^i < b_{n,n+1}^{ii} < b_{n,n+1}^i < b_{n+1}^{ii} < \ldots \uparrow -1$$

(where $b_{1,2}^i = O(|\log\varepsilon|)$) at which additional pairs of $2n-1$ or $2n$-pulse homoclinic orbits are created (see figures 5, 6, 7). These bifurcations are called *first* bifurcations since they are surrounded by (exponentially close) higher order homoclinic saddle-node bifurcations (Theorem 6.8). However, these results do not give a complete description of the full complexity of the intersection $W^{\rm s}(\Gamma) \cap W^{\rm u}(\Gamma)$ in the counteracting case. This is discussed in section 7. Here we also relate the distinction between the cooperating and the counteracting case to a similar distinction that is responsible for the existence of various types

of homoclinic explosions and implosions as described in [5] (see also [2] for a proof of the existence of homoclinic explosions and implosions in a Ginzburg-Landau system).

As mentioned above, the motivation to study these sequences of homoclinic bifurcations in (1.1) is based on the observation that homoclinic and heteroclinic orbits to (1.5) correspond to traveling localized structures in the family of modulation equations (1.3). But, from the viewpoint of the theory of dynamical systems, we study in this paper a simple global co-dimension 1 phenomenon that will occur in large classes of three-dimensional nearly integrable systems. We have introduced the second parameter, b, to distinguish between two clearly different cases: the one in which the slow flow (along Γ) and the (averaged) fast flow 'cooperate' and the much more complicated one in which the fast flow 'counteracts' the slow flow. The approach of the analysis in this paper is mainly geometrical and does not rely on a specific form of the model system. This includes the quantitative results (Theorems 4.2, 5.1): these are also based on a geometrical singular perturbation theory ([8], [15], [13], [12]). This approach enabled us to unravel much of the complex structure of $W^{\rm s}(\Gamma) \cap W^{\rm u}(\Gamma)$ in (1.1). Due to the nature of the analysis in this paper, it is likely that a similar complexity can be observed in a more general class of singularly perturbed systems.

Remark 1.1 The homoclinic saddle-node bifurcation studied in this paper has also been observed – but not analysed – in [2]. Here heteroclinic and homoclinic solutions to a system of the type (1.5), derived from a Ginzburg-Landau equation with a small quintic term, are studied in a fashion similar to the analysis in [5] and this paper. The manifolds $W^{\rm s}(\Gamma)$ and $W^{\rm u}(\Gamma)$ are tangent on the (two-dimensional) bifurcation manifold $\mathcal{C}_t$ (in a three-dimensional parameter space). However, in this problem there are also other, structurally different, mechanisms that create or annihilate intersections of $W^{\rm s}(\Gamma)$ and $W^{\rm u}(\Gamma)$.

Remark 1.2 The structure of this paper is as follows: in section 2 we apply Fenichel, Melnikov and averaging theory to determine some fundamental properties of (1.1). In section 3 we prove some basic lemmas that will be used throughout the paper. The geometrical analysis of the cooperating case is presented in section 4, the quantitative aspects are considered in section 5. Section 6 is devoted to the counteracting case. The paper is concluded with a short discussion.

2 The model problem

We define the integral of (1.1) with $\varepsilon = 0$ as

$$k = \frac{1}{2}y^2 - \frac{1}{2}x^2 + \frac{1}{3}x^3. \tag{2.1}$$

For $\varepsilon = 0$ the manifold $\{x = 1, y = 0\}$ consisting of center points corresponds to $k = -\frac{1}{6}$, the line $\{x = 0, y = 0\}$ of saddles and the homoclinic manifold $\mathcal{H}$ correspond to $k = 0$. Inside $\mathcal{H}$ a family of invariant cylinders filled with periodic orbits exists. The manifold $\mathcal{H}$ consists of a family of homoclinic orbits

$$x(t) = \frac{3}{2}\mathrm{sech}^2(\frac{1}{2}t),\ y(t) = \dot{x}(t),\ z(t) = z_0 \tag{2.2}$$

See also Figure 1.

According to Fenichel (see [8] and, for instance, [12]), the perturbed system has a hyperbolic slow manifold $\Gamma, O(\varepsilon)$ close to $\{x = 0, y = 0\}$, within each compact neighbourhood of $\{x = 0, y = 0, |z| \leq C\}$ for arbitrary $C \in \mathbf{R}$. Clearly, in this case $\Gamma = \{x = 0, y = 0\}$, since $\{x = 0, y = 0\}$ is still a hyperbolic invariant manifold for $\varepsilon > 0$.

Again by Fenichel theory, for $\varepsilon > 0$, Γ has stable and unstable manifolds $O(\varepsilon)$ close to those of the unperturbed case (consider a region which is closed and bounded with respect to z). Let $W^{\mathrm{s}}(\Gamma)$ respectively $W^{\mathrm{u}}(\Gamma)$ denote those components of the stable and unstable manifolds which lie $O(\varepsilon)$ close to the manifold $\mathcal{H}$ for $t \gg 0$ (respectively $t \ll 0$).

To use Fenichel theory and to derive and apply some lemmas in section 3 we will (often) need that z is in some compact region. Without disturbing the essential ingredients of the model system, we therefore put two saddle points 'far away' on Γ:

$$(2.3) \qquad \begin{cases} \dot{x} &= y \\ \dot{y} &= x - x^2 + \varepsilon y(z^2 - a) \\ \dot{z} &= \varepsilon(1 + bx - cz^2), \end{cases}$$

with $1 \gg c \gg \varepsilon$. However, for our geometrical arguments in sections 4-6 it is more convenient to use the first system. All arguments can be applied to system (2.3) as well; see for instance Remark 4.1. Note that the parameter c in (2.3) is fixed in contrast with the bifurcation parameters a and b.

2.1 Some basic definitions

Define the first intersections of $W^{\mathrm{u}}(\Gamma)$ and $W^{\mathrm{s}}(\Gamma)$ with $\{y = 0\}$, lying $O(\varepsilon)$ close to the component $\{y = 0, x = \frac{3}{2}\}$ of $\mathcal{H} \cap \{y = 0\}$, by $P(\Gamma)$ respectively $P^{-1}(\Gamma)$.

We say that $P(\Gamma)$ lies *inside* $W^{\mathrm{s}}(\Gamma)$ for z in some region when $p < s$ for points $(p, 0, z) \in P(\Gamma)$ and $(s, 0, z) \in P^{-1}(\Gamma) \subset W^{\mathrm{s}}(\Gamma)$. Similarly, $P(\Gamma)$ lies *outside* $W^{\mathrm{s}}(\Gamma)$ when $s < p$. These definitions are also used for $P^{-1}(\Gamma)$ and $W^{\mathrm{u}}(\Gamma)$.

In Figure 2 the manifolds Γ, $W^{\mathrm{s}}(\Gamma)$ and $W^{\mathrm{u}}(\Gamma)$, and the intersection curves $P(\Gamma)$ and $P^{-1}(\Gamma)$ are sketched. In section 2.2 we will explain why this figure corresponds to values $a > 0$.

2.2 Melnikov theory

We use the Melnikov method for slowly varying systems to obtain an expression for the distance as a function of z between $W^{\mathrm{u}}(\Gamma)$ and $W^{\mathrm{s}}(\Gamma)$. In fact, we measure the distance between their first intersections $P(\Gamma)$ and $P^{-1}(\Gamma)$ with $\{y = 0, x > 1\}$. Since the homoclinic orbits are intersections of $W^{\mathrm{u}}(\Gamma)$ and $W^{\mathrm{s}}(\Gamma)$, we can detect them with this instrument.

Points $x^{\mathrm{u}}_\varepsilon$ and $x^{\mathrm{s}}_\varepsilon$ are defined as the intersections of $P(\Gamma)$ (respectively. $P^{-1}(\Gamma)$) with $\{z = z_0\}$. Solutions $\gamma^{\mathrm{u}}_\varepsilon = (x^{\mathrm{u}}_\varepsilon, y^{\mathrm{u}}_\varepsilon, z^{\mathrm{u}}_\varepsilon)$ in $W^{\mathrm{u}}(\Gamma)$ and $\gamma^{\mathrm{s}}_\varepsilon = (x^{\mathrm{s}}_\varepsilon, y^{\mathrm{s}}_\varepsilon, z^{\mathrm{s}}_\varepsilon)$ in $W^{\mathrm{s}}(\Gamma)$ of equations (1.1) or (2.3) are determined by the initial condition $\gamma^{\mathrm{u,s}}_\varepsilon(0) = (x^{\mathrm{u,s}}_\varepsilon, 0, z_0)$ and $\gamma_0(t) =$

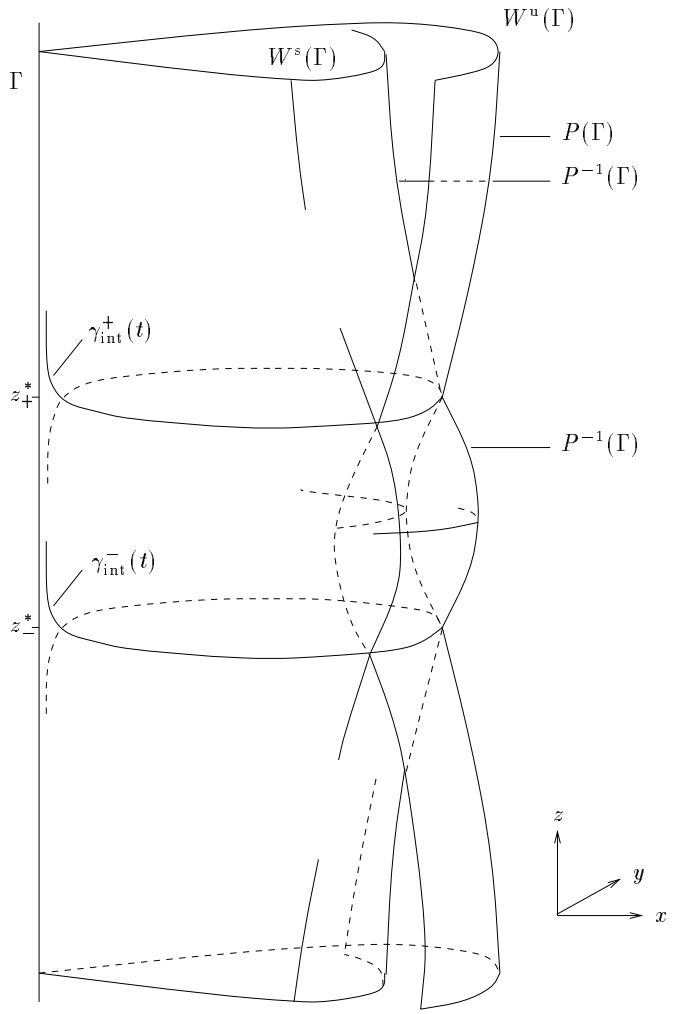

Figure 2: The structure of $W^{\mathrm{s}}(\Gamma)$ and $W^{\mathrm{u}}(\Gamma)$ and their first intersections $P^{-1}(\Gamma)$ respectively $P(\Gamma)$ with the plane $\{y = 0\}$ for $a > 0$. Note that $P(\Gamma)$ is inside $W^{\mathrm{s}}(\Gamma)$ for $z \in (z^{*}_{-}, z^{*}_{+})$ and outside $W^{\mathrm{s}}(\Gamma)$ for all other z.

$(x_0(t), y_0(t), z_0)$ is defined as the homoclinic solution to the unperturbed system ($\varepsilon = 0$) with $\gamma_0(0) = (\frac{3}{2}, 0, z_0)$. We define the following time-dependent weighted distance function:

$$\triangle W(t, z_0) = \begin{pmatrix} y_0(t) \\ x_0(t) - x_0^2(t) \end{pmatrix} \wedge \begin{pmatrix} \frac{\partial}{\partial \varepsilon}[x_\varepsilon^{\mathbf{u}}(t) - x_\varepsilon^{\mathbf{s}}(t)]\,|_{\varepsilon=0} \\ \frac{\partial}{\partial \varepsilon}[y_\varepsilon^{\mathbf{u}}(t) - y_\varepsilon^{\mathbf{s}}(t)]\,|_{\varepsilon=0} \end{pmatrix},$$

which is the same for systems (1.1) and (2.3).

Using the expression for the Melnikov function derived in [18] (see also [21]) we find

$$\begin{aligned} \triangle W(0, z) &= \int_{-\infty}^{\infty} \begin{pmatrix} y_0(t) \\ x_0(t) - x_0^2(t) \end{pmatrix} \wedge \begin{pmatrix} 0 \\ y_0(t)(z_0^2 - a) \end{pmatrix} dt \\ &= \int_{-\infty}^{\infty} y_0^2(t)(z_0^2 - a) dt \qquad (2.4) \\ &= \frac{6}{5}(z^2 - a). \end{aligned}$$

Hence, $\triangle W(0, z) = 0$ for $z = \pm\sqrt{a}$ if $a \geq 0$ and $\triangle W(0, z) \neq 0$ for all z if $a < 0$. Therefore, varying the parameter a gives us the global saddle-node bifurcation described in the introduction.

The function $\triangle W(0, z; a)$ measures the $O(\varepsilon)$ distance between $P(\Gamma)$ and $P^{-1}(\Gamma)$. The derivatives of $W^{\mathbf{u}}(\Gamma)$ and $W^{\mathbf{s}}(\Gamma)$ are controlled by Fenichel's Second Invariant Manifold Theorem (see [12]). Thus a simple zero z_0 of $\triangle W(0, z; a)$ defines exactly one transversal intersection point $P(\Gamma) \cap P^{-1}(\Gamma)$; its position is $O(\varepsilon)$ close to the point $(\frac{3}{2}, 0, z_0)$. We define $z_\pm^* = \pm\sqrt{a} + O(\varepsilon)$ as the exact z values for which $P(\Gamma)$ and $P^{-1}(\Gamma)$ intersect (see Figure 2).

For the moment we define by $D(z; a, \varepsilon)$ the *exact* weighted distance between $P(\Gamma)$ and $P^{-1}(\Gamma)$. Then $D(z; a, \varepsilon) = \triangle W(0, z; a) + \varepsilon f(z; a, \varepsilon)$. Applying the Implicit Function Theorem on $\frac{\partial}{\partial z} D(z; a, \varepsilon) = \frac{12}{5} z + \varepsilon \frac{\partial}{\partial z} f(z; a, \varepsilon)$ one obtains for every $\varepsilon_0 > 0$, small enough, a unique value $z_0(\varepsilon_0)$ such that $\frac{\partial}{\partial z} D(z_0; a, \varepsilon_0) = 0$ and hence the function $D(z; a, \varepsilon)$ has a unique minimum, given by $m = \frac{6}{5}(z_0^2 - a) + \varepsilon_0 f(z_0; a, \varepsilon_0)$. Since the $O(1)$ part of this expression is linear in a and $\frac{\partial m}{\partial a} = O(1)$ with respect to ε, there is exactly one value of a, such that this minimum is zero. For this value $a^*(\varepsilon_0)$, $P(\Gamma)$ and $P^{-1}(\Gamma)$ are exactly tangent. From now on, we will say that $P(\Gamma)$ and $P^{-1}(\Gamma)$ are tangent for $a = a^*$ in a point with z coordinate z^*. Obviously $a^* = 0 + O(\varepsilon)$, since $\triangle W(0, z)$ has a double zero for $a = 0$ exactly.

Remark 2.1 The expression $\triangle W(0, z; a)$ measures the distance between the *first* intersections of $W^{\mathbf{u}}(\Gamma)$ and $W^{\mathbf{s}}(\Gamma)$ (or $P(\Gamma)$ and $P^{-1}(\Gamma)$) with the $\{y = 0\}$-plane. Below we refer to intersections of $P(\Gamma)$ and $P^{-1}(\Gamma)$ as primary intersection points (see also [5]). In this paper we will consider all possible intersections of $W^{\mathbf{u}}(\Gamma)$ and $W^{\mathbf{s}}(\Gamma)$. Note that a Melnikov-function for higher order intersections has recently been developed in [19] and [1]. However, we still find that our geometric approach gives (many) more intersections $W^{\mathbf{u}}(\Gamma) \cap W^{\mathbf{s}}(\Gamma)$ than predicted by these Melnikov-functions (see also Remark 4.6 and especially section 6).

Furthermore, as mentioned, we distinguish between the cooperating and the counteracting case. The difference between these cases is related to the z direction of the 'averaged' flow in the fast field, so we need a measure for this flow.

The flow inside the manifolds $W^{\mathrm{s}}(\Gamma)$ and $W^{\mathrm{u}}(\Gamma)$ is studied by a Poincaré map on the cross section $\{y = 0, 1 < x < \frac{3}{2} + O(\varepsilon)\}$:

$$\mathcal{P}(k, z) = (k + \triangle K(k, z),\ z + \triangle Z(k, z))$$

with k as in (2.1), $k \in (-\frac{1}{6}, 0)$. The Poincaré map $\mathcal{P}$ is well defined since the flow starting at the cross section is $O(\varepsilon)$ close to the periodic or homoclinic orbits of the unperturbed system. Note, however, that there are points on the boundary of this cross section for which $\mathcal{P}$ is not defined. We will repeatedly apply this map on $P(\Gamma)$ and $P^{-1}(\Gamma)$, and we therefore define for $n > 1$:

$$\begin{array}{ll} P^n(\Gamma) & \equiv \mathcal{P}^{n-1}(P(\Gamma)), \\ P^{-n}(\Gamma) & \equiv \mathcal{P}^{-n+1}(P^{-1}(\Gamma)). \end{array} \tag{2.5}$$

Note that there is a difference between P in $P(\Gamma)$ and $\mathcal{P}$: P corresponds to half of the Poincaré map $\mathcal{P}$ which is defined above, while P^n corresponds to applying P once, followed by applying $\mathcal{P}$ $n-1$ times.

The quantities $\triangle K(k, z)$ and $\triangle Z(k, z)$ measure the accumulated change in the variables k and z of a solution $(x_\varepsilon(t), y_\varepsilon(t), z_\varepsilon(t))$, with initial data on the cross section $\{y = 0, x \geq 1\}$, at its first return to this cross section after a time $T_\varepsilon(k, z)$. Thus,

$$\triangle K(k, z) = \int_0^{T_\varepsilon(k,z)} \dot{k}(x_\varepsilon, y_\varepsilon, z_\varepsilon)dt = \varepsilon \int_0^{T_\varepsilon(k,z)} y_\varepsilon^2(z_\varepsilon^2 - a)dt,$$

and

$$\triangle Z(k, z) = \int_0^{T_\varepsilon(k,z)} \dot{z}(x_\varepsilon, y_\varepsilon, z_\varepsilon)dt = \varepsilon \int_0^{T_\varepsilon(k,z)} (1 + bx_\varepsilon - cz_\varepsilon^2)dt.$$

We approximate $(x_\varepsilon(t), y_\varepsilon(t), z_\varepsilon(t))$ and T_ε by $(x_0(t), y_0(t), z_0(t))$ and T_0, the solution with period T_0 of system (2.3) with $\varepsilon = 0$ and the same or $O(\varepsilon)$ close initial data and obtain

$$\triangle K(k, z_0) = \varepsilon \int_0^{T_0(k,z_0)} y_0(t)^2(z_0^2 - a)dt + O(\varepsilon^2), \tag{2.6}$$

$$\triangle Z(k, z_0) = \varepsilon \int_0^{T_0(k,z_0)} (1 + bx_0(t) - cz_0^2)dt + O(\varepsilon^2). \tag{2.7}$$

After changing variables these expressions become

$$\triangle K(k, z) = 2\varepsilon \int_{x_1(k)}^{x_2(k)} (z^2 - a)\sqrt{2k + x^2 - \frac{2}{3}x^3}\, dx + O(\varepsilon^2),$$

$$\triangle Z(k, z) = 2\varepsilon \int_{x_1(k)}^{x_2(k)} \frac{1 + bx - cz^2}{\sqrt{2k + x^2 - \frac{2}{3}x^3}} dx + O(\varepsilon^2) \tag{2.8}$$

Here $0 < x_1(k) < 1 < x_2(k) < \frac{3}{2}$ are the intersection points with $\{y = 0\}$ of the unperturbed orbit.

We compute estimates on $\triangle Z(k,z)$ with $|z| \ll \frac{1}{\sqrt{c}}$ in the limit $k \downarrow -\frac{1}{6}$ and for $|k| \ll 1$ by the methods presented in [5]:

$$\lim_{k\downarrow -\frac{1}{6}} \triangle Z(k,z) = 2\varepsilon\pi(1+b) + O(\varepsilon c) + O(\varepsilon^2),$$

$$\triangle Z(k,z) = -\varepsilon \log|k| + 6\varepsilon b + \text{h.o.t., when } |k| \ll 1. \tag{2.9}$$

The estimates for $|z| \ll \frac{1}{\sqrt{c}}$ are sufficient since in the following we will study the bifurcation at $a = a^*$ for which only an $O(1)$ neighbourhood of the $\{z = 0\}$-plane is important. For system (1.1) we do not need the constraint $|z| \ll \frac{1}{\sqrt{c}}$.

Furthermore, we observe from (2.6) that

$$\triangle K(0,z) = \varepsilon \int_{-\infty}^{\infty} y_0^2(t)(z^2 - a)dt + O(\varepsilon^2) = \frac{6}{5}\varepsilon(z^2 - a) + O(\varepsilon^2). \tag{2.10}$$

Note from (2.4) and (2.10) that $\triangle W(0,z)$ and $\triangle K(0,z)$ are essentially the same:

$$\triangle K(0,z) = \varepsilon \triangle W(0,z) + O(\varepsilon^2).$$

Thus, the weighted distance $D(z; a, \varepsilon)$ introduced in this section corresponds to measuring the distance with respect to the integral k.

We now turn back to the distinction between the two different cases. The system is called *cooperating* if the averaged flow of orbits in the fast field is in the same z direction as, and thus cooperates with, the flow on Γ:

$$\triangle Z(k,z) > 0.$$

For $b \geq 0$ the system obviously satisfies this condition (see (2.8: $|z| \leq \frac{1}{\sqrt{c}}$). The bifurcation gets more complicated if the averaged flow in the z-direction caused by the fast field *counteracts* the slow field, so if

$$\triangle Z(k,z) < 0$$

for some k. Clearly, the influence of the slow manifold Γ on orbits close to the axis $\{x = 1, y = 0\}$ is much less – but we will find not always negligible – than on orbits close to the stable and unstable manifolds. Therefore, we expect that this condition is easier satisfied for $x \to 1$, $y \to 0$ (so $k \downarrow -\frac{1}{6}$), than for $k \ll 1$, $k > 0$. By (2.8) and (2.9) this can be shown rigorously: for $b < -1$, we might have a small counteracting region, a neighbourhood of $\{x = 1, y = 0\}$, while $\triangle Z(k,z)|_{\{0<k\ll 1\}} < 0$ will only be satisfied for $b = O(-\log\varepsilon)$, $b < 0$.

3 Quantitative aspects

3.1 A lemma on $\mathcal{P}$ and $\mathcal{P}^{-1}$

To detect intersections of $W^{\mathrm{u}}(\Gamma)$ and $W^{\mathrm{s}}(\Gamma)$ we will repeatedly apply the Poincaré map $\mathcal{P}$ respectively $\mathcal{P}^{-1}$ on $P(\Gamma)$ resp. $P^{-1}(\Gamma)$, and look for intersections $P^n(\Gamma) \cap P^{-m}(\Gamma)$ (see (2.5)). Since $\triangle W(k,z) = \frac{6}{5}(z^2 - a)$, the distance between $P(\Gamma)$ and $P^{-1}(\Gamma)$ is $O(\varepsilon)$ as long as $z = O(1)$. To understand how $\mathcal{P}$ resp. $\mathcal{P}^{-1}$ act on $P(\Gamma)$ resp. $P^{-1}(\Gamma)$, we thus only have to know the effect of these maps on points at a distance $\delta = O(\varepsilon)$, or less, from $P^{-1}(\Gamma)$ (if $P(\Gamma)$ lies inside $W^{\mathrm{s}}(\Gamma)$) respectively $P(\Gamma)$ (if $P^{-1}(\Gamma)$ lies inside $W^{\mathrm{u}}(\Gamma)$).

We therefore use the following lemma:

Lemma 3.1 *If $d(q_0, P^{-1}(\Gamma)) = \delta \ll 1$ for a point $q_0 = (x,y,z)$ with $k(q_0) < 0 + O(\varepsilon)$, then $d(\mathcal{P}(q_0), P(\Gamma)) = O(\delta)$. Similarly, if $d(q_0, P(\Gamma)) = \delta$ for a point $q_0 = (x,y,z)$ with $k(q_0) < 0 + O(\varepsilon)$, then $d(\mathcal{P}^{-1}(q_0), P^{-1}(\Gamma)) = O(\delta)$.*

Here $d(.,.)$ is the standard distance function or, equivalently and in the same order of magnitude with respect to ε, the weighted distance expressed in the integral values k.

To prove this lemma, we follow a solution $\gamma_0(t)$ of (2.3) with $\gamma_0(t_0) = q_0 = (x_0, 0, z_0)$, where $1 < x_0 < \frac{3}{2} + O(\varepsilon)$. We assume that this solution returns to the plane $\{y = 0, 1 < x < \frac{3}{2} + O(\varepsilon)\}$ at $t = t_1$ in the point $\mathcal{P}(q_0)$. The trajectory of $\gamma_0(t)$ is divided into three parts. The second one gives the local behaviour of $\gamma_0(t)$ in a neighbourhood $\mathcal{B}$ of Γ and the other two describe its behaviour outside this neighbourhood.

In particular, the box $\mathcal{B}$ is determined by the Fenichel normal form for the system and the behaviour inside it is found by studying this normal form (see [12]). We begin by deriving this Fenichel normal form for equation (2.3). The eigenvalues for the linearization about a point $(x,y,z) = (0,0,z_0)$ are

$$\begin{aligned} \lambda_0 &= 0 - 2\varepsilon c z_0 + O(\varepsilon^3) \\ \lambda_\pm &= \pm 1 + \tfrac{1}{2}(z_0^2 - a)\varepsilon + O(\varepsilon^2). \end{aligned}$$

Using the corresponding eigenvectors as new coordinate axes, we define the variables

$$\begin{aligned} \xi &= x + \lambda_+ y + \tfrac{\varepsilon b}{\lambda_+ + 2\varepsilon c z_0} z, \\ \eta &= x + \lambda_- y + \tfrac{\varepsilon b}{\lambda_- + 2\varepsilon c z_0} z. \end{aligned}$$

The third variable, z, remains the same. Equations (2.3) can now be written as

$$\begin{cases} \dot{\xi} = \lambda_+ \xi + f_1(\xi, \eta, z, \varepsilon) \\ \dot{\eta} = \lambda_- \eta + f_2(\xi, \eta, z, \varepsilon) \\ \dot{z} = \varepsilon(1 + bx(\xi, \eta, z, \varepsilon) - cz^2)) \end{cases}$$

in a neighbourhood $\hat{\mathcal{B}}$ of Γ with $|z| \leq \sqrt{\frac{1}{c}}$. Here the functions f_1 and f_2 are C^r functions representing nonlinear terms in ξ and η and linear terms in ξ and η that are $O(\varepsilon)$.

We use one more change of coordinates to straighten out the local stable and unstable manifolds such that they can be used as coordinate axes. According to Fenichel (see for

instance [12]) for any $r > 0$ there exist C^r functions $s(\eta, z, \varepsilon)$ and $u(\xi, z, \varepsilon)$, defined for ξ and η in $\hat{\mathcal{B}}$, such that the invariant manifolds $W^{\mathrm{s}}(\Gamma)$ and $W^{\mathrm{u}}(\Gamma)$ are given by the sets

$$\{\xi = s(\eta, z, \varepsilon)\} \text{ and } \{\eta = u(\xi, z, \varepsilon)\}$$

within the neighbourhood $\hat{\mathcal{B}}$ of Γ. The functions s and u satisfy the properties $s(0, z, \varepsilon) = 0$, $u(0, z, \varepsilon) = 0$, $\frac{\partial s}{\partial \eta}(0, z, \varepsilon) = 0$ and $\frac{\partial u}{\partial \xi}(0, z, \varepsilon) = 0$. If we define the coordinate transformation

$$(p, q) = (\xi - s(\eta, z, \varepsilon), \eta - u(\xi, z, \varepsilon))$$

then (1.1) takes the form

$$\begin{cases} \dot{p} = \lambda_+ p + F_1(p, q, z, \varepsilon)p \\ \dot{q} = \lambda_- q + F_2(p, q, z, \varepsilon)q \\ \dot{z} = \varepsilon(1 + bx(p, q, z, \varepsilon) - cz^2). \end{cases} \tag{3.1}$$

within $\hat{\mathcal{B}}$. Clearly $\{p = 0\}$ and $\{q = 0\}$ are the local invariant manifolds. The functions F_i contain linear and higher order terms in p and q, as well as $O(\varepsilon)$ terms. To simplify further computations we define a neighbourhood $\mathcal{B} \subset \hat{\mathcal{B}}$ of Γ with $\mathcal{B} = \{(p, q, z) : |p| \leq \Delta, |q| \leq \Delta, |z| \leq \sqrt{\frac{1}{c}}\}$ for some $1 \gg \Delta \gg \varepsilon > 0$ small enough, and the normal form will be applied in this neighbourhood.

Outside $\mathcal{B}$ we write the system as $\dot{v} = g(v)$, with $v = (x, y, z)$ and

$$g(v) = g(x, y, z) = \begin{pmatrix} y \\ x - x^2 + \varepsilon(z^2 - a) \\ \varepsilon(1 + bx - cz^2) \end{pmatrix}$$

Proof of Lemma 3.1: First we show, that solutions which start at a distance δ from $P^{-1}(\Gamma)$ remain $O(\delta)$ close to $W^{\mathrm{s}}(\Gamma)$ outside $\mathcal{B}$ and hence enter $\mathcal{B}$, at time $t = t_{\mathrm{in}}$, $O(\delta)$ close to $W^{\mathrm{s}}(\Gamma)$. Considering the time-reversed vector field, one can analogously show, that solutions starting at a distance δ from $P(\Gamma)$ will enter $\mathcal{B}$ at $O(\delta)$ distance from $W^{\mathrm{u}}(\Gamma)$. In other words, a solution which leaves $\mathcal{B}$ at time $t = t_{\mathrm{out}}$ $O(\delta)$ close to $W^{\mathrm{u}}(\Gamma)$ will hit the plane $\{y = 0\}$ at time $t = t_1$ $O(\delta)$ close to $P(\Gamma)$.

The proof will then be completed by showing that a solution which enters $\mathcal{B}$ at an $O(\delta)$ distance from $W^{\mathrm{s}}(\Gamma)$ leaves this box $O(\delta)$ close to $W^{\mathrm{u}}(\Gamma)$.

We define solutions $\gamma_s(t)$ and $\gamma_u(t)$ on $W^{\mathrm{s}}(\Gamma)$ and $W^{\mathrm{u}}(\Gamma)$ respectively. The solution $\gamma_s(t)$ is chosen such that $\|\gamma_s(t_0) - \gamma_0(t_0)\| = \|\gamma_s(t_0) - q_0\| = \delta$. The solutions satisfy $\dot{\gamma}_s = g(\gamma_s)$ and $\dot{\gamma}_0 = g(\gamma_0)$, so $\dot{\gamma}_s - \dot{\gamma}_0 = g(\gamma_s) - g(\gamma_0)$. After integrating and taking norms we get:

$$\|\gamma_s(t) - \gamma_0(t)\| \leq \|\gamma_s(t_0) - \gamma_0(t_0)\| + \int_{t_0}^{t} \|g(\gamma_s(\tau)) - g(\gamma_0(\tau))\| d\tau. \tag{3.2}$$

By the mean value theorem, we have

$$\|g(\gamma_s(\tau)) - g(\gamma_0(\tau))\| \leq L\|\gamma_s(\tau) - \gamma_0(\tau)\| \tag{3.3}$$

for some L (and $v = (x, y, z)$ in a compact region Ω). Now, the combination of (3.2) and (3.3), with $\|\gamma_s(t_0) - \gamma_0(t_0)\| = \delta$ yields, by Gronwall's lemma,

$$\|\gamma_s(t) - \gamma_0(t)\| \leq \delta e^{\int_{t_0}^{t} L d\tau} = \delta e^{L(t-t_0)}.$$

We can conclude that, as long as $0 < L(t-t_0) < N$, where N is some constant independent of δ, $\|\gamma_s(t) - \gamma_0(t)\| = O(\delta)$. Such N exists, since the solutions spend only $O(1)$ time with respect to ε in the fast field.

Therefore, $\|\gamma_s(t_{\text{in}}) - \gamma_0(t_{\text{in}})\| = O(\delta)$ and hence the solution enters $\mathcal{B}$ $O(\delta)$ close to $W^{\text{s}}(\Gamma)$.

As mentioned above, the same result can be obtained for the other part of $\gamma_0(t)$ outside $\mathcal{B}$ by applying these arguments on $\gamma_0(t)$ and $\gamma_u(t)$.

For the proof inside $\mathcal{B}$ we consider the equations (3.1). The linear and higher order terms in p and q contained in F_i, $i = 1, 2$, are of order Δ. Besides these terms, F_i also contain $O(\varepsilon)$ terms, so $F_i = O(\Delta, \varepsilon)$ for $i = 1, 2$. Hence, since z remains $O(1)$ inside $\mathcal{B}$, we can rewrite (3.1) as:

$$\begin{cases} \dot{p} = (\lambda_+ + O(\Delta, \varepsilon))p \\ \dot{q} = (\lambda_- + O(\Delta, \varepsilon))p \\ \dot{z} = O(\varepsilon). \end{cases} \tag{3.4}$$

The initial conditions for p and q are given by $q(t_{\text{in}}) = q_{\text{in}} = \Delta$, $p(t_{\text{in}}) = p_{\text{in}} = O(\delta)$ and $z(t_{\text{in}}) = z_{\text{in}} = z_0 + O(\delta, \varepsilon)$, which follows from the Gronwall estimates from above. Furthermore, $p(t_{\text{out}}) = p_{\text{out}} = \Delta$.

We now compute $q_{\text{out}} = q(t_{\text{out}})$ by integrating (3.4):

$$\begin{pmatrix} p_{\text{out}} \\ q_{\text{out}} \end{pmatrix} = \begin{pmatrix} \Delta \\ q_{\text{out}} \end{pmatrix} = \begin{pmatrix} O(\delta)\, e^{(\lambda_+ + O(\Delta,\varepsilon))(t_{\text{out}} - t_{\text{in}})} \\ \Delta e^{(\lambda_- + O(\Delta,\varepsilon))(t_{\text{out}} - t_{\text{in}})} \end{pmatrix} \tag{3.5}$$

For the moment, we write $\tau = t_{\text{out}} - t_{\text{in}}$. Since $\lambda_+ = -\lambda_-(1 + O(\varepsilon))$, we can substitute $e^{\lambda_+ t} = e^{-\lambda_- t(1+O(\varepsilon))} = e^{-\lambda_- t}(1 + O(\varepsilon t))$ into (3.5) to obtain:

$$p_{\text{out}} = \Delta = O(\delta)\, e^{-\lambda_- \tau}(1 + O(\varepsilon\tau))(1 + O(\Delta, \varepsilon)\tau),$$

which implies by (3.5):

$$\begin{aligned} q_{\text{out}} &= \Delta e^{(\lambda_- + O(\Delta,\varepsilon))\tau} = \Delta e^{\lambda_- \tau}(1 + O(\Delta, \varepsilon)\tau) \\ &= O(\delta)(1 + O(\varepsilon\tau))(1 + O(\Delta, \varepsilon)\tau)^2 \\ &= O(\delta), \end{aligned} \tag{3.6}$$

since $\tau = t_{\text{out}} - t_{\text{in}} \leq O(\frac{1}{\varepsilon})$ by the assumption that z remains $O(1)$ in $\mathcal{B}$. Combining the results for the three parts of the trajectory of $\gamma_0(t)$ we obtain the desired result: the

distance between $\mathcal{P}(q_0)$ and $P(\Gamma)$ is $O(\delta)$ if the distance between q_0 and $P^{-1}(\Gamma)$ is δ and $k(q_0) < 0 + O(\varepsilon)$ (this means that q_0 lies at the left side of $P^{-1}(\Gamma)$). The second case of the lemma is proved similarly, considering the time-reversed vector field. □

Some results in this proof can be used to obtain an estimate for the difference in z between a point q_0 on the cross section, lying at a distance δ from $P^{-1}(\Gamma)$, and its image $\mathcal{P}(q_0)$. This is formulated in the following lemma, that will be useful in the next sections.

Lemma 3.2 *For the solution starting in $q_0 \in \{y = 0, x > 1\}$ at time $t = t_0$ the time of flight T that is needed to return to the half plane $\{y = 0, x > 1\}$ satisfies*

$$T = O(|\log \delta|);$$

during this time T the z coordinate of the solution increases with an amount

$$\triangle z(q_0) = O(\varepsilon |\log \delta|),$$

if $d(q_0, P^{-1}(\Gamma)) = \delta$ with $|\log \delta| \ll \frac{1}{\varepsilon}$.

Proof: The trajectory followed by the solution through q_0 was divided into three parts. The two parts outside the box $\mathcal{B}$ take $O(1)$ time. Combining (3.5) and (3.6), we find

$$q_{\text{out}} = \Delta e^{(\lambda_- + O(\Delta,\varepsilon))(t_{\text{out}} - t_{\text{in}})} = O(\delta).$$

The time of flight inside $\mathcal{B}$ is found by solving this equation:

$$t_{\text{out}} - t_{\text{in}} = O(|\log \delta|),$$

provided that $|\log \delta| \ll \frac{1}{\varepsilon}$. Hence, the total time T can be estimated by

$$T = O(|\log \delta|).$$

By $\dot{z} = \varepsilon(1 + bx - cz^2)$ (2.3) we know that, during a time T, the z coordinate of a solution will increase with an amount $\triangle z = O(\varepsilon T) + \text{h.o.t.}$. Here we use that $b = O(1)$, and that x and z do not grow without bound. For $T = O(|\log \delta|)$, this implies

$$\triangle z(q_0) = O(\varepsilon |\log \delta|).$$

□

3.2 Behaviour close to the stable and unstable manifolds

Another result we will apply several times follows from a lemma which we copy from the proof of the 'exchange lemma with exponentially small error' in [13]: In the following, we denote by $\mathcal{B}$ the compact neighbourhood of Γ defined in section 3.1, which allows us to use Fenichel coordinates (3.1). Furthermore, l is a constant satisfying $0 < l < 1$, so $0 < l < \lambda_+$ and $\lambda_- < -l < 0$, where $\lambda_- = -1$, $\lambda_+ = 1$ are the stable and unstable eigenvalues of the unperturbed system , respectively.

Lemma 3.3 *Let $(p(t), q(t), z(t))$ be a solution of (3.1). There exist constants $c_p, c_q, c, K > 0$ such that, for $s \leq t$*

1. $|q(t)| \leq c_q |q(s)| e^{-l(t-s)}$,

2. $|p(t)| \geq c_p |p(s)| e^{l(t-s)}$,

3. $\int_s^t |p(\zeta)||q(\zeta)| d\zeta \leq K e^{c(s-t)}$,

independently of ε, *where* $K = 2\Delta^2 \max(\frac{1}{c_p l}, \frac{c_q}{l})$ *and* $c = \frac{l}{2}$, *so long as the trajectory stays in* $\mathcal{B}$.

This lemma can be interpreted as follows:

Lemma 3.4 *If the* p *coordinate at which a solution enters* $\mathcal{B}$ *is in an appropriate (exponentially small) range, while* $|q| = \Delta$, *the trajectory of this solution remains in* $\mathcal{B}$ *for an* $O(\frac{1}{\varepsilon})$ *time and leaves* $\mathcal{B}$ *at a point of the form* $|p| = \Delta$ *with* $|q|$ *exponentially small.*

Between the entrance in $\mathcal{B}$ *and the departure from* $\mathcal{B}$ *there is a time interval of length* $O(\frac{1}{\varepsilon})$ *such that* $|p|$ *and* $|q|$ *are exponentially small for all times* t *in this interval. During this time interval the solution follows the slow manifold closely and hence the* z *coordinate changes with an* $O(1)$ *amount.*

4 Geometrical analysis of the cooperating case

We analyse the form and intersections of $W^{\mathrm{u}}(\Gamma)$ and $W^{\mathrm{s}}(\Gamma)$ and the global bifurcations by studying the intersections of the two manifolds with the halfplane $\{y = 0, x > 1\}$.

In this and following sections we will repeatedly apply the quantitative arguments based on system (2.3) (Lemmas 3.1, 3.2 and 3.4) . However, for our geometrical arguments it does not matter if the z coordinate remains bounded or not, so for convenience we use the original system (1.1).

Remark 4.1 In the geometric analysis we will frequently state that a point p has an image $\mathcal{P}(p)$, respectively a preimage $\mathcal{P}^{-1}(p)$, at ∞ with respect to z, respectively at $-\infty$. This means that the orbit through p remains exponentially close to Γ for all positive, respectively negative, t, i.e. the orbit through p is homoclinic to Γ. The corresponding behaviour in system (2.3) can be described as follows:

This system has two saddle points on Γ, one with positive (S^+) and one with negative z coordinate (S^-). The point S^+ has a two-dimensional stable manifold $W^{\mathrm{s}}(S^+)$ and a one-dimensional strong unstable manifold $W^{\mathrm{u}}(S^+)$, while S^- has a two-dimensional unstable manifold $W^{\mathrm{u}}(S^-)$ and a one-dimensional strong stable manifold $W^{\mathrm{s}}(S^-)$. Hence the orbit through a point $p \in P^{-1}(\Gamma)$ is homoclinic to Γ for $t \to \infty$ if it tends to S^+. Orbits through points exponentially close to p will be mapped by $\mathcal{P}$ to a neighbourhood of $W^{\mathrm{u}}(S^+) \cap P^{-1}(\Gamma)$ (instead of a point with z coordinate $\gg 1$ as in system (1.1)).

Similarly, an orbit homoclinic to Γ for $t \to -\infty$ in system (1.1) corresponds to an orbit coming out of S^- (see [5] and [9] for a detailed description of the maps $\mathcal{P}$ and $\mathcal{P}^{-1}$ near critical points on Γ).

4.1 After the bifurcation

We consider the cooperating case ($b > -1$) after the appearance of the first pair of homoclinic orbits that are created by the saddle-node bifurcation at $a = a^* = 0 + O(\varepsilon)$.

Note that the first two created 1-pulse homoclinic orbits, $\gamma^+_{\rm int}(t)$ and $\gamma^-_{\rm int}(t)$, are orbits homoclinic to Γ, however, in system (2.3) they should also be interpreted as heteroclinic orbits between S^- and S^+. These orbits are called 1-pulse orbits since they only make one circuit through the fast field (see Figure 2).

First we describe the structures of sets $W^{\rm u}(\Gamma) \cap \{y = 0\} = \bigcup_{n\geq 1} P^{-n}(\Gamma)$ and $W^{\rm s}(\Gamma) \cap \{y = 0\} = \bigcup_{n\geq 1} P^{n}(\Gamma)$ as $a > a^*$ and $a = O(1)$, i.e. the two intersection points $\gamma^+_{\rm int}(0) = (x_+, 0, z^*_+)$ and $\gamma^-_{\rm int}(0) = (x_-, 0, z^*_-) \in P(\Gamma) \cap P^{-1}(\Gamma)$ lie $O(1)$ from each other. We exclude the possibility of counteracting slow and fast fields, since such fields imply more homoclinic orbits as we will find in section 6.

Below we formulate a theorem on the existence of N-pulse homoclinic orbits. An N-pulse homoclinic orbit is defined as an orbit that makes N circuits through the fast field. Such orbits are associated to intersections of $P(\Gamma)$ and $P^{-N}(\Gamma)$. Note that we can restrict ourselves to the intersections $P(\Gamma) \cap P^{-N}(\Gamma)$ since other intersections as $P^n(\Gamma) \cap P^{-m}(\Gamma)$ also correspond to an $N = n + m - 1$-pulse homoclinic orbit described by the intersection $P(\Gamma) \cap P^{-N}(\Gamma)$. (This can be seen by applying the Poincaré map $\mathcal{P}^{-1}$ $(n-1)$ times to the point $P^n(\Gamma) \cap P^{-m}(\Gamma)$.)

Theorem 4.2 *When $a > 0$, $a = O(1)$, and $b \geq -1$, there are* two *N-pulse homoclinic orbits for all $N \leq O(|\log \varepsilon|)$. For each such N, one of the N-pulse orbits has all its N fast excursions near the $\{z = z^*_+\}$-plane and the other one makes its first excursion near the plane $\{z = z^*_-\}$ and all other $(N-1)$ excursions near the $\{z = z^*_+\}$-plane.*

The geometrical arguments in the following two subsections form the main part of the proof this theorem. In section 5 the proof is completed by some quantitative results.

All qualitative results on the phase space of this system are indicated in Figure 3.

4.1.1 Images of $P(\Gamma)$

The Poincaré map $\mathcal{P}$ defined in section 2.2 is only well defined for points on $P(\Gamma)$ with $x < \frac{3}{2} + \varepsilon$, so for the part of $P(\Gamma)$ which lies inside $W^{\rm s}(\Gamma)$. Thus, the parts of $P(\Gamma)$ outside $W^{\rm s}(\Gamma)$, i.e. with z coordinate $z < z^*_-$ or $z > z^*_+$, have no image under $\mathcal{P}$. In the same way $\mathcal{P}^{-1}$ is valid for the part of $P^{-1}(\Gamma)$ lying inside $W^{\rm u}(\Gamma)$. By Lemma 3.1 and Lemma 3.2 points $p = (x, 0, z)$ with $z^*_- < z < z^*_+$ on $P(\Gamma)$ have images $\mathcal{P}(p)$ lying $O(\varepsilon)$ from $P(\Gamma)$ and $O(|\varepsilon \log \varepsilon|)$ higher than p with respect to the z coordinate, provided that p does not lie exponentially close to $P^{-1}(\Gamma)$. Thus, the second intersection $P^2(\Gamma) \equiv \mathcal{P}(P(\Gamma))$ of $W^{\rm u}(\Gamma)$ with the Poincaré cross section $\{y = 0, x > 1\}$ partly lies $O(\varepsilon)$ to the left of $P(\Gamma)$. (See Figure 3.)

However, the orbit through a point p_1 on $P(\Gamma)$, exponentially close to and below $\gamma^+_{\rm int}(0)$ with respect to z enters a neighbourhood of Γ and leaves this neighbourhood exponentially close to $W^{\rm u}(\Gamma)$ according to Lemma 3.4. Thus its next intersection with $\{y = 0, x > 1\}$ is exponentially close to $P(\Gamma)$. The closer p_1 is to $\gamma^+_{\rm int}(0)$, the more the orbit is 'stretched' due to the upward direction of the flow on the slow manifold. We can conclude that $P^2(\Gamma)$ partly lies exponentially close to $P(\Gamma)$ and is unbounded in the $+z$ direction.

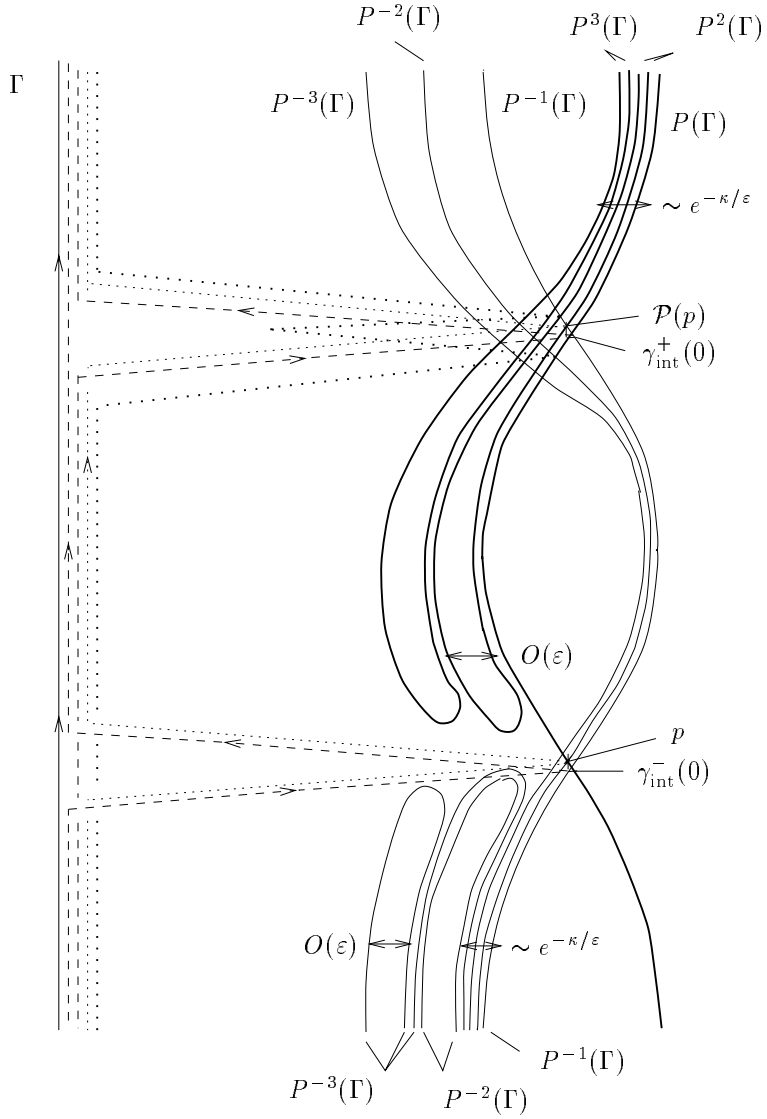

Figure 3: The global structure of $W^{\rm u}(\Gamma)$ and $W^{\rm s}(\Gamma)$ in the cooperating case for $a > 0$ and $O(1)$ shown via intersection with the plane $\{y = 0\}$. The 1-pulse homoclinic orbits, $\gamma^+_{\rm int}(t)$, $\gamma^-_{\rm int}(t)$ and the 2-pulse homoclinic orbits have been added as 'schematic projections' , respectively as - - - and $\cdots$. The points p and $\mathcal{P}(p)$ denote two intersection points $P(\Gamma) \cap P^{-2}(\Gamma)$ and $P^2(\Gamma) \cap P^{-1}(\Gamma)$ corresponding to the same 2-pulse homoclinic orbit.

Lemma 3.4 can also be applied to an orbit through a point p_2 exponentially close to and above $\gamma^-_{\rm int}(0)$. Again, the image $\mathcal{P}(p_2)$ lies higher and exponentially close to $P(\Gamma)$. Therefore, $P^2(\Gamma)$ is an $O(\varepsilon)$ thick tongue which extends to infinity and becomes exponentially thin in the $+z$ direction.

Note that this description is only accurate for system (1.1). In system (2.3) both unbounded parts of $P^2(\Gamma)$ will remain bounded, but with a large $(O(\frac{1}{\sqrt{c}}))$ z coordinate: they are 'stitched' to the point $W^{\rm u}(S^+) \cap \{y = 0\}$ (see [5], [9]). As already said in Remark 4.1, we will not distinguish any longer between the structures of $P^N(\Gamma)$, $(N = \pm 1, \pm 2, \ldots)$ for $|z| \gg 1$. Our descriptions are based on system (1.1).

We now apply the Poincaré map on $P^2(\Gamma)$, i.e. the part of $P^2(\Gamma)$ that lies at the inside of $W^{\rm s}(\Gamma)$. Since $P^2(\Gamma)$ contains points in the region $z^*_- < z < z^*_+$ and has two continuous and unbounded branches in the $+z$ direction, it has two transversal intersection points with $P^{-1}(\Gamma)$, corresponding with two 2-pulse homoclinic orbits. Using the above arguments one can see that points p_3 on $P^2(\Gamma)$ close to and below $P^2(\Gamma) \cap P^{-1}(\Gamma)$ have images exponentially close to $P(\Gamma)$ with z coordinates increased by the influence of the slow manifold Γ. The part of $P^2(\Gamma)$ not too close to the intersection points $P^2(\Gamma) \cap P^{-1}(\Gamma)$ is only mapped over an $O(\varepsilon)$ distance (with respect to x) by $\mathcal{P}$.

Summarizing these observations we see, that the image $\mathcal{P}(P^2(\Gamma)) = P^3(\Gamma)$ is just a copy of $P^2(\Gamma)$. Repeating these arguments gives a structure of many tongues $P^n(\Gamma)$ that become exponentially thin for large values of z . In section 5 we will show that there are $O(|\log \varepsilon|)$ of such tongues for $a > 0$ and $O(1)$.

4.1.2 Preimages of $P^{-1}(\Gamma)$

We apply $\mathcal{P}^{-1}$ several times to deduce the global structure of $W^{\rm s}(\Gamma)$. Note that $\mathcal{P}^{-1}$ is only defined inside $W^{\rm u}(\Gamma)$. A point q_1 on $P^{-1}(\Gamma)$ above but not too close to $\gamma^+_{\rm int}(0)$ is mapped $O(\varepsilon)$ to the left by $\mathcal{P}^{-1}$ according to Lemma 3.1. By Lemma 3.4, a point q_2 close above $\gamma^+_{\rm int}(0)$ has its preimage exponentially close to $P^{-1}(\Gamma)$ and much lower than q_2. Therefore, the part of $P^{-1}(\Gamma)$ above $\gamma^+_{\rm int}(0)$ is mapped by $\mathcal{P}^{-1}$ to a branch $P^{-2}(\Gamma)$ which is unbounded in both z directions.The distance between $P^{-1}(\Gamma)$ and $P^{-2}(\Gamma)$ is $O(\varepsilon)$ for $z > z^*_+$ and exponentially small for $z \ll z^*_+$. See Figure 3.

Remark 4.3 Surely, a certain part of $P^{-2}(\Gamma)$ with $z^*_- < z < z^*_+$ lies exponentially close to $P^{-1}(\Gamma)$ since points in this region are preimages of points on $P^{-1}(\Gamma)$ in a neighbourhood of $\gamma^+_{\rm int}(0)$. However, we do not know anything about the distance between $P^{-1}(\Gamma)$ and $P^{-2}(\Gamma)$ in a neighbourhood of $\gamma^+_{\rm int}(0)$ yet. In section 5 we present some quantitative results on this distance.

Since the branch $P^{-2}(\Gamma)$ intersects $P(\Gamma)$ above $\gamma^+_{\rm int}(0)$, $P^{-2}(\Gamma)$ contains points arbitrarily close to the intersection of a 2-pulse homoclinic orbit and $\{y = 0\}$. Combining Lemma 3.1 for points on $P^{-2}(\Gamma)$ far enough from an intersection point and Lemma 3.4 for points exponentially close to $P^{-1}(\Gamma)$, we can thus conclude that $P^{-3}(\Gamma)$ contains a branch like this $P^{-2}(\Gamma)$-branch. Inductively, a structure of many analogous branches $P^{-n}(\Gamma)$ is obtained.

Orbits through points on $P^{-1}(\Gamma)$ with $z < z_-^*$ behave for decreasing time like those on $P(\Gamma)$ with $z_-^* < z < z_+^*$ for increasing time: the largest part of $P^{-1}(\Gamma)$ is mapped $O(\varepsilon)$ to the inside, while points close to and below $\gamma_{\rm int}^-(0)$ return exponentially close to $P^{-1}(\Gamma)$. This way, an $O(\varepsilon)$ thick tongue arises which does not have any intersection points with $W^{\rm u}(\Gamma)$. See Remark 4.4 below. Thus, $P^{-2}(\Gamma)$ consists of two disjoint parts (see Figure3. Applying $\mathcal{P}^{-1}$ again, we see that $P^{-3}(\Gamma)$ contains a tongue similar to the $P^{-2}(\Gamma)$-tongue.

So far we constructed two disjoint parts of $P^{-3}(\Gamma)$. However, $P^{-3}(\Gamma)$ also has a third component: the image of that part of $P^{-2}(\Gamma)$ that is exponentially close to $P^{-1}(\Gamma)$ and that is below, with respect to the z coordinate, $\gamma_{\rm int}^-(0)$. This part of $P^{-2}(\Gamma)$ is mapped to a second tongue $P^{-3}(\Gamma)$ folded exponentially close around the $P^{-2}(\Gamma)$ tongue since it is the preimage of a part of $P^{-2}(\Gamma)$ that is exponentially close to $P^{-1}(\Gamma)$. Hence, $P^{-3}(\Gamma)$ consists of three components. Applying $\mathcal{P}^{-1}$ repeatedly, we conclude that $P^{-4}(\Gamma)$ consists of four disjoint parts, $P^{-5}(\Gamma)$ of five parts, etc.

Each branch $P^{-N}(\Gamma)$ has two intersection points with $P(\Gamma)$, one near $\{z = z_-^*\}$ and one near $\{z = z_+^*\}$, both corresponding with an N-pulse homoclinic orbit. All other intersections $P^n(\Gamma) \cap P^{-m}(\Gamma)$ lie in the neighbourhood of $\{z = z_+^*\}$ and correspond with these homoclinic orbits as noted above. We thus proved Theorem 4.2 except for the quantitative statement on N. This will be done in section 5.

The behaviour of different homoclinic orbits and the connection between different intersection points $P^n(\Gamma) \cap P^{-m}(\Gamma)$ can be understood using the intersections $W^{\rm u,s}(\Gamma) \cap \{y = 0, x > 1\}$ and applying Lemmas 3.1 and 3.4. In Figure 3 the two primary homoclinic orbits are drawn, together with the 2-pulse orbit which has both pulses near the plane $\{z = z_+^*\}$ and the 2-pulse orbit which makes its first excursion through the fast field near the plane $\{z = z_-^*\}$.

Remark 4.4 The tongues of $P^{-2}(\Gamma)$, $P^{-3}(\Gamma)$, etc. cannot intersect the $P^2(\Gamma)$, $P^3(\Gamma)$, ...-tongues. This is a simple consequence of the fact that we restricted ourselves to the cooperating case: the z coordinate of the image of a point p under $\mathcal{P}$ has always increased, while the z coordinate of the preimage of point q under $\mathcal{P}^{-1}$ has always decreased.

In section 6 we will consider the counteracting case: decreasing b below -1 creates many new intersections of the $P^n(\Gamma)$ and $P^{-m}(\Gamma)$ tongues.

Remark 4.5 The structures of $W^{\rm u}(\Gamma)$ and $W^{\rm s}(\Gamma)$ can also be studied by studying the intersections of $W^{\rm u}(\Gamma)$ and $W^{\rm s}(\Gamma)$ with a plane $\{z = \text{const.}\}$. Instead of applying Lemmas 3.1, 3.2 and 3.4 one then uses the Lambda Lemma (see for instance [9], [21]) to deduce the structure of $W^{\rm u}(\Gamma) \cap \{z = \text{const.}\}$ and $W^{\rm s}(\Gamma) \cap \{z = \text{const.}\}$. Although these two approaches of course yield the same structures for $W^{\rm u}(\Gamma)$ and $W^{\rm s}(\Gamma)$, we found that the above approach is a more convenient one. In [5] both approaches have been considered.

Remark 4.6 In [19] Soto-Treviño and Kaper developed and used a higher order Melnikov method to detect N-pulse homoclinic orbits, but when applying their method on system (1.1) one only finds one zero $z = z_+^* + O(\varepsilon)$ for each adiabatic Melnikov function $M_{N,A}(z, \varepsilon)$ which satisfies the conditions of their Theorem 1, i.e. this Melnikov method only detects one of the two N-pulse homoclinic orbits. This can be understood by realizing that this method (and likewise the Melnikov method described in [1]) can by construction not describe orbits that come exponentially close to Γ. Thus, the N-pulse orbit that makes one

circuit near the $\{z = z_-^*\}$-plane and all other circuits near the $\{z = z_+^*\}$-plane cannot be found by these Melnikov methods. Note however that Kaper and Soto-Treviño also made a remark on this phenomenon and use geometric arguments similar to the ones mentioned in Remark 4.5 to describe it.

4.2 The bifurcations

The constructions in the previous section enable us to study the first homoclinic saddle-node bifurcation at $a = a^*$ and the following saddle-node bifurcations at which the N-pulse homoclinic orbits are constructed. The main results about the bifurcation are formulated in the following theorem:

Theorem 4.7 *Let a^* be the parameter value such that the stable and unstable manifolds $W^s(\Gamma)$ and $W^u(\Gamma)$ of Γ are tangent in $\gamma_{\rm int}(t)$ for $a = a^*$; $W^s(\Gamma)$ and $W^u(\Gamma)$ intersect in two primary homoclinic orbits for $a > a^*$ and have no primary intersections for $a < a^*$. Then:*

1. *For $a = a^*$ the orbit $\gamma_{\rm int}(t)$ is the* only *homoclinic orbit to Γ. For $a < a^*$, $W^u(\Gamma)$ and $W^s(\Gamma)$ do not intersect at all.*

2. *There exists a sequence of parameter values a_n^* with $a_{n+1}^* > a_n^*$, $n > 1$, at which two n-pulse homoclinic orbits are created in a saddle-node bifurcation.*

The distance between successive bifurcations a_n^* and a_{n+1}^* will be estimated in section 5.

Proof: To describe the bifurcation, we start with the situation for $a = a^*$ and then consider values $a < a^*$ and $a > a^*$ with $|a - a^*|$ small.

For $a = a^*$ the Poincaré map $\mathcal{P}^{-1}$ is well defined for all points on $P^{-1}(\Gamma)$. The intersection point $\gamma_{\rm int}(0)$ is mapped by $\mathcal{P}^{-1}$ to $-\infty$ with respect to the z coordinate and thus orbits through points on $P^{-1}(\Gamma)$ exponentially close to $\gamma_{\rm int}(0)$ return to $\{y = 0\}$ at a large negative z coordinate and exponentially close to $P^{-1}(\Gamma)$, by the influence of the slow manifold (Lemma 3.4). The preimages of these points form two branches $P^{-2}(\Gamma)$. Most of $P^{-1}(\Gamma)$ however is only mapped $O(\varepsilon)$ to the left and $O(\varepsilon \log \varepsilon)$ downwards by Lemma 3.1. Since the preimage of the point $\gamma_{\rm int}(0)$ is the only discontinuity in $P^{-2}(\Gamma)$, the branch with preimages of points close to, but above, $\gamma_{\rm int}(0)$ is connected with the preimages of higher (with respect to z) points. The branch of preimages of points under $\gamma_{\rm int}(0)$ forms a tongue as in Figure 4(b).

In section 5 we will prove that the distance between $P^{-2}(\Gamma)$ and $P(\Gamma)$ is big enough to assume that the influence of Γ is topologically negligible for orbits through points on $P^{-2}(\Gamma)$. Thus we conclude that $P^{-3}(\Gamma)$ and following preimages simply are $O(\varepsilon)$ shifts of $P^{-2}(\Gamma)$ as shown in Figure 4(b).

If a increases towards a^*, then the distance between $P(\Gamma)$ and $P^{-1}(\Gamma)$ becomes eventually exponentially small. Thus some points on $P^{-1}(\Gamma)$ are already mapped downwards by $\mathcal{P}^{-1}$ (by the slow flow on Γ) and have preimages exponentially close to $P^{-1}(\Gamma)$ according to Lemma 3.4. There is a point on $P^{-1}(\Gamma)$ closest to $\gamma_{\rm int}(0)$, so there is an orbit which is stretched most and defines a local minimum for $P^{-2}(\Gamma)$. Hence, $P^{-2}(\Gamma)$ forms a thin tongue exponentially close to $P^{-1}(\Gamma)$. See Figure 4(a). The z coordinate of its local

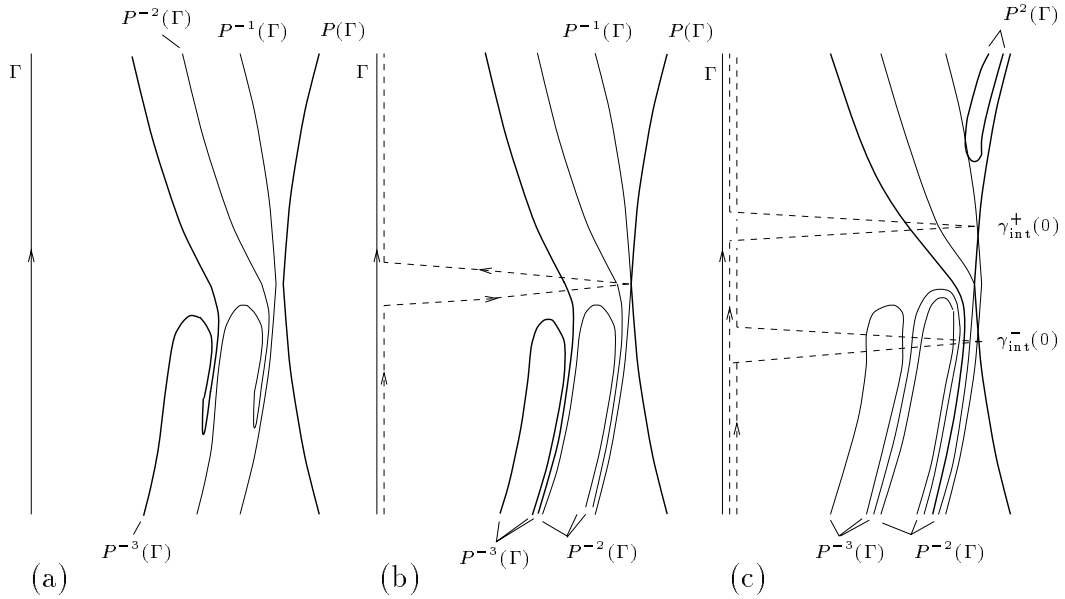

Figure 4: Global structures of $W^{\rm u}(\Gamma)$ and $W^{\rm s}(\Gamma)$ shown via intersections with $\{y = 0, x > 1\}$; (a) $a < a^*$, $|a - a^*|$ small, (b) $a = a^*$, (c) $a > a^*$ small, $a = a_2^*$. Besides two primary intersection points there are two tangent intersections in (c) (of $P^2(\Gamma)$ and $P^{-1}(\Gamma)$ and of $P(\Gamma)$ and $P^{-2}(\Gamma)$) corresponding to the same 2-pulse homoclinic orbit.

minimum becomes more negative if a comes closer to $a = a^*$. Again the branches $P^{-n}(\Gamma)$ are $O(\varepsilon)$ shifts of $P^{-1}(\Gamma)$. Note that $P^n(\Gamma) = \emptyset$ for $n > 1$ as long as $a \leq a^*$. This proves the first statement of Theorem 4.7.

As a increases and passes $a = a^*$ the branches $P^{-n}(\Gamma)$ start to intersect $P(\Gamma)$ one after another. Define the parameter values a_n^* as the value of a for which $P^{-n}(\Gamma)$ and $P(\Gamma)$ are tangent. Still, the distance between successive branches is big enough (see again section 5), which means that the influence of Γ on a branch $P^{-n-1}(\Gamma)$ is negligible when $a = a_n^*$.

As soon as $a > a^*$ there is a (little) part of $P(\Gamma)$ inside $P^{-1}(\Gamma)$, thus $P^2(\Gamma)$ has become non-empty. If $a - a^* = O(e^{\frac{-\kappa}{\varepsilon}})$ for some constant κ, then all points on $P(\Gamma)$ for which $\mathcal{P}$ is defined are exponentially close to $P^{-1}(\Gamma)$: their images have a 'large' z coordinate. In other words, as a passes through a^*, a little $P^2(\Gamma)$-tongue appears with $z \gg 1$. This tongue comes down to $z \approx z^*$ very rapidly: it is already tangent to $P^{-1}(\Gamma)$ (near $\gamma^+_{\rm int}(0)$) when the branch $P^{-2}(\Gamma)$ is tangent to $P(\Gamma)$ (see Figure 4(c)). Following the homoclinic orbits it is easy to see, that an intersection $P(\Gamma) \cap P^{-2}(\Gamma)$ implies that the tongue $P^2(\Gamma)$ intersects $P^{-1}(\Gamma)$. A little $P^3(\Gamma)$-tongue appears as a passes a_2^*, since the tongue $P^2(\Gamma)$ starts to intersect $P^{-1}(\Gamma)$ at $a = a_2^*$ and there is a part of $P^2(\Gamma)$ inside $P^{-1}(\Gamma)$ for $a > a_2^*$.

In the same way, every next intersection $P(\Gamma) \cap P^{-n}(\Gamma)$ implies that a tongue $P^n(\Gamma)$ intersects $P^{-1}(\Gamma)$ and that intersections of tongues $P^k(\Gamma)$ with $P^{k-n}(\Gamma)$ must exist. The reverse holds also: each intersection of a tongue $P^m(\Gamma)$ with some branch $P^{-n}(\Gamma)$ immediately implies other intersections. This can also be seen by applying $\mathcal{P}$ $n-1$ times on an intersection point $\mathcal{P}^{-n+1}(P(\Gamma)) \cap P(\Gamma) = P^{-n}(\Gamma) \cap P(\Gamma)$.

Also, every next intersection $P(\Gamma) \cap P^{-n}(\Gamma)$ implies that the next exponentially thin tongue $P^{-n-1}(\Gamma)$, which appeared when $P^{-n}(\Gamma)$ reached $P(\Gamma)$ close enough, becomes infinitely deep. This concludes the proof of Theorem 4.7. □

When a increases, $P(\Gamma)$ only needs a short time to pass branches $P^{-n}(\Gamma)$, but it is clear that the N-pulse orbits are created one by one, and not in an explosion, as in [5]. The distance, or time, between successive bifurcations will be estimated in section 5. Note that we thus arrive at the situation described by Theorem 4.2 and sketched in Figure 3 as a has become $O(1)$.

5 The distance between successive bifurcations

In section 4.2 we showed qualitatively, that N-pulse homoclinic orbits are created one by one in a sequence of 'nearby' bifurcations. This section considers the corresponding quantitative aspects: we estimate the distance between successive bifurcations.

Theorem 5.1 *Let a_n^* be as in Theorem 4.7 with $n = O(1)$. Then the distance between successive bifurcations a_n^* and a_{n+1}^* is given by*

$$a_{n+1}^* - a_n^* = O(\varepsilon^2(\log \varepsilon)^2).$$

In order to determine this distance we use the distance d between branches $P^{-n}(\Gamma)$ and $P^{-n-1}(\Gamma)$ at height $z = z^* = 0 + O(\varepsilon)$. Clearly, this distance satisfies $O(e^{-\frac{K}{\varepsilon}}) \ll d \ll O(\varepsilon)$, since the distance between branches $P^{-n}(\Gamma)$ and $P^{-n-1}(\Gamma)$ measured in a plane $\{z = \bar{z}\}$ is $O(\varepsilon)$ for $\bar{z} \to \infty$ and $O(e^{-\frac{K}{\varepsilon}})$ for $\bar{z} \to -\infty$.

Proof: We start with a point p_1 on $P^{-2}(\Gamma)$ with $z = z^*$, as in Figure 5. The distance $d(p_1, P^{-1}(\Gamma))$ between p_1 and $\gamma_{\text{int}}(0)$ is defined as d_1, where $d(.,.)$ is standard distance function. Then by Lemma 3.1 we know that the distance between the image $\mathcal{P}(p_1)$ and $P(\Gamma)$ is $O(d_1)$. Another instrument to measure this distance is the Melnikov function, or, equivalently, $\triangle K$ (see section 2). We combine the expressions obtained by the two different methods to get an estimate for d_1.

First note that if we take two points x_1 and x_2 on $\{y = 0, x > 1\}$ and define $k_{1,2} = k(x_{1,2}, 0)$ (see (2.1)), then for $0 < \delta \ll 1$

$$|x_1 - x_2| = O(\delta) \Leftrightarrow |k_1 - k_2| = O(\delta)$$

as long as $|k_i + \frac{1}{6}| = O(\varepsilon)$, i.e. as long as $(x_i, 0)$ are not too close to the center points of the unperturbed system. Thus, the distance $d = O(\delta)$ is equivalent to $\triangle K(0, z) = O(\delta)$.

To be able to use the Melnikov function, one needs to know the z coordinate of $\mathcal{P}(p_1)$. By Lemma 3.2 we have $\triangle z(p_1) = O(-\varepsilon \log d_1)$, so this z coordinate is given by $z = z^* + O(-\varepsilon \log d_1)$.

However, filling in this expression in the Melnikov function $\triangle W(0, z)$ or, equivalently, in $\triangle K(0, z) = \frac{6}{5}\varepsilon(z^2 - a) + O(\varepsilon^2)$, one sees that higher order terms are needed, since the only information about the distance d_1 is $d_1 = O(\varepsilon)$ (or less). From (2.6) we recall that

$$\triangle K(k, z) = \varepsilon \int_0^{T_\varepsilon(k,z)} y_\varepsilon^2(t)(z_\varepsilon^2(t) - a)dt.$$

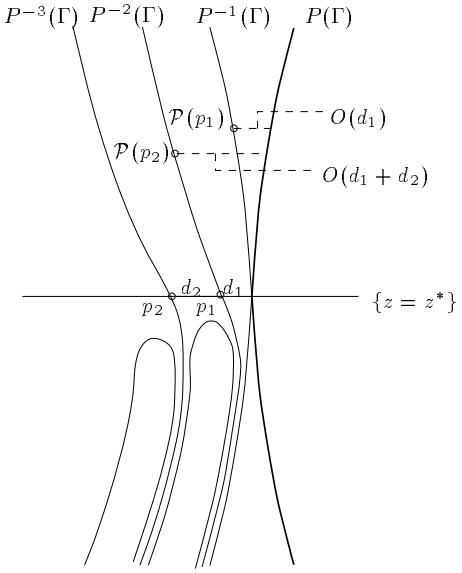

Figure 5: Distance between successive branches $P^{-n}(\Gamma)$ when $a = a^*$.

Since we are interested in solutions on the perturbed stable and unstable manifolds the interval of integration $(0, T_\varepsilon(k,z))$ must be replaced by $(-\infty, \infty)$. We expand the solutions $(x_\varepsilon(t), y_\varepsilon(t), z_\varepsilon(t))$ of (1.1) in powers of ε:

$$\begin{aligned} x_\varepsilon(t) &= x_0(t) + \varepsilon x_1(t) + \varepsilon^2 x_2(t) + \text{ h.o.t.} \\ y_\varepsilon(t) &= y_0(t) + \varepsilon y_1(t) + \varepsilon^2 y_2(t) + \text{ h.o.t.} \\ z_\varepsilon(t) &= z_0 + \varepsilon z_1(t) + \varepsilon^2 z_2(t) + \text{ h.o.t.} \end{aligned} \tag{5.1}$$

as $\varepsilon \to 0$, where $(x_0(t), y_0(t), z_0)$ is an unperturbed homoclinic solution (see (2.2)). Filling in these expansions yields

$$\begin{aligned} \triangle K(0, z_0, a) &= \varepsilon \int_{-\infty}^{\infty} y_0^2(t)(z_0^2 - a)dt \\ &\quad + \varepsilon^2 \int_{-\infty}^{\infty} (2y_0^2(t) z_0 z_1(t) + 2z_0^2 y_0(t) y_1(t))dt + O(\varepsilon^3). \end{aligned} \tag{5.2}$$

By substituting (5.1) into (1.1) , we find for the first-order correction of z:

$$z_1(t) = z_1(0) + \int_0^t (1 + b x_0(\tau))d\tau. \tag{5.3}$$

The symmetry in the unperturbed system yields that $x_0(t)$ is an even function. Hence $z_1(t)$ is odd if $z_1(0) = 0$, which can be obtained by imposing $z_\varepsilon(0) = z_0$.

The term $y_1(t)$ is bounded for all t. Also, $y_0(t)$ goes to zero exponentially fast for $t \to \pm\infty$, since this term corresponds with the unperturbed orbit (2.2) which approaches the hyperbolic fixed point $(0, 0, z_0)$. Hence, the improper integral $\int_{-\infty}^{\infty} y_0(t) y_1(t) dt$ converges absolutely and we can put

$$I = \int_{-\infty}^{\infty} y_0(t) y_1(t) dt.$$

As a result we have, taking into account that the first term in the second integral of (5.2) is odd:

$$(5.4) \qquad \triangle K(0, z_0, a) = \frac{6}{5}\varepsilon(z_0^2 - a) + 2I\varepsilon^2 z_0^2 + O(\varepsilon^3).$$

For notational convenience, we denote the z coordinate of a point $\mathcal{P}^m(p_n)$ by $z_{n,m}$. Equation (5.4) for $z = z_{1,1}$ and $a = a^*$ gives, using a Taylor expansion around $z = z^*$:

$$\begin{aligned}\triangle K(0, z_{1,1}, a^*) &= \triangle K(0, z^*, a^*) + \tfrac{\partial(\triangle K)}{\partial z}\big|_{z=z^*}(z_{1,1} - z^*) \\ &\quad + \tfrac{1}{2}\tfrac{\partial^2(\triangle K)}{\partial z^2}\big|_{z=z^*}(z_{1,1} - z^*)^2 + \text{ h.o.t.} \\ &= (\tfrac{12}{5}\varepsilon z^* + 4I\varepsilon^2 z^*)O(-\varepsilon \log d_1) \\ &\quad + (\tfrac{12}{5}\varepsilon + 4I\varepsilon^2)O(\varepsilon^2(\log d_1)^2) + \text{ h.o.t.},\end{aligned}$$

since $|z_{1,1} - z^*| = O(-\varepsilon \log d_1)$. After filling in $z^* = 0 + O(\varepsilon)$ (see section 2) this leads to

$$\triangle K(0, z_{1,1}, a^*) = O(\varepsilon^3(\log d_1)^2).$$

As noted above, Lemma 3.1 yields that $d(\mathcal{P}(p_1), P(\Gamma)) = d_1$; thus, $d_1 = O(\varepsilon^3(\log d_1)^2)$ and hence

$$d_1 = O(\varepsilon^3(\log \varepsilon)^2)$$

in the sense of the following remark.

Remark 5.2 The equation $d_1 = O(\varepsilon^3(\log d_1)^2)$ requires, that d_1 does not contain higher or lower powers of ε than ε^3, since $\varepsilon^{3+\sigma} < O(\varepsilon^3(\log \varepsilon^{3+\sigma})^2)$ and $\varepsilon^{3-\sigma} > O(\varepsilon^3(\log \varepsilon^{3-\sigma})^2)$ for all $\sigma > 0$. Thus, $d_1 = \varepsilon^3|\log \varepsilon|^\alpha +$ h.o.t.. Filling in this expression in the equation for d_1, we obtain $\varepsilon^3|\log \varepsilon|^\alpha = O(\varepsilon^3(\log(\varepsilon^3|\log \varepsilon|^\alpha))^2)$, where we surely have $\varepsilon^3|\log \varepsilon|^\alpha = d_1 \in (\varepsilon^{3+\sigma}, \varepsilon^{3-\sigma})$ in the right term for all $\sigma > 0$. This yields $\varepsilon^3|\log \varepsilon|^\alpha \sim O(\varepsilon^3(3 \pm \sigma)^2|\log \varepsilon|^2)$, which gives $\alpha = 2$ as a first estimate. Now d_1 cannot contain higher or lower powers of $\log \varepsilon$ than $(\log \varepsilon)^2$, so $d_1 = \varepsilon^3(\log \varepsilon)^2 C$, where C contains loglog-like terms, etc.

Now consider a point p_2 on $P^{-3}(\Gamma)$ with z coordinate z^*, with $d(p_1, p_2) = d_2$ (see Figure 5) and thus with $d(p_2, P^{-1}(\Gamma)) = d_1 + d_2$. The z coordinate of its image $\mathcal{P}(p_2)$ is $z_{2,1} = z^* + \triangle z(p_2) = z^* - \varepsilon \log(d_1 + d_2)$. According to Lemma 3.1 the distance between $\mathcal{P}(p_2)$ and $P(\Gamma)$ at this height is $O(d_1 + d_2) = O(\varepsilon^3(\log \varepsilon)^2) + O(d_2)$, which is equal to $\triangle K(0, z^* - \varepsilon \log(d_1 + d_2), a^*) + d(\mathcal{P}(p_2), P^{-1}(\Gamma))$. By (5.4) we have $\triangle K(0, z^* - \varepsilon \log(d_1 + d_2), a^*) = O(\varepsilon^3(\log(d_1 + d_2))^2)$.

Lemma 3.1 also implies, that a horizontal segment which has a width δ when it enters the neighbourhood $\mathcal{B}$ of Γ leaves this neighbourhood as a segment still of width $O(\delta)$. Since such segment remains its width in $O(1)$ time, this yields that the distance $d(\mathcal{P}(p_1), \mathcal{P}(p_2))$ (and also $d(\mathcal{P}(p_2), P^{-1}(\Gamma))$) is of the same order ($O(d_2)$) as $d(p_1, p_2)$. As a result the distance between $\mathcal{P}(p_2)$ and $P(\Gamma)$ is $O(\varepsilon^3(\log d_1)^2) + O(d_2) = O(\varepsilon^3(\log(d_1 + d_2))^2) + O(d_2)$. This leads to $d_1 + d_2 = O(d_1)$:

$$d_2 = O(\varepsilon^3(\log \varepsilon)^2).$$

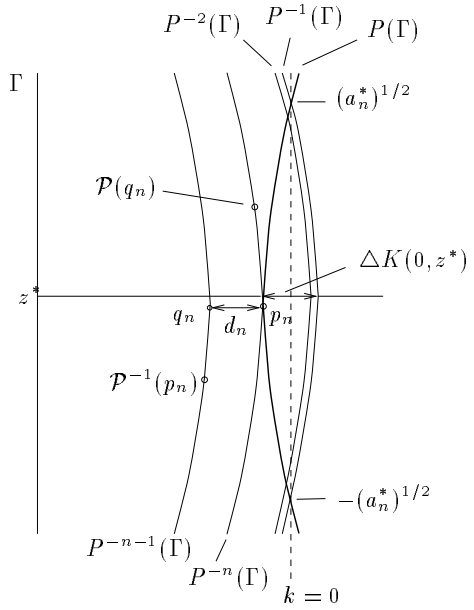

Figure 6: Intersections of $W^{\rm u}(\Gamma)$ and $W^{\rm s}(\Gamma)$ with the plane $\{y=0, x>1\}$ for $a = a_n^* \gg \varepsilon^2(\log\varepsilon)^2$.

This process can be continued by taking a point p_3 on $P^{-4}(\Gamma)$ with z coordinate z^*, with $d(p_3,p_2) = d_3$ and thus with $d(p_3, P^{-1}(\Gamma)) = d_1 + d_2 + d_3$, etc. As a result, all branches $P^{-n}(\Gamma)$ (where $n = O(1)$) lie $O(\varepsilon^3(\log\varepsilon)^2)$ close to each other. Since the lowest order terms of $\triangle K$ depend on a linearly, $\triangle K(0,z,a_1) - \triangle K(0,z,a_2) = O(\varepsilon(a_1-a_2))$. For $a_1 = a^*$ and $a_2 = a_2^*$ this means that $\triangle K(0,z^*,a_2^*) = d_1 = O(\varepsilon^3(\log\varepsilon)^2)$ and thus

$$a_2^* = a^* + O(\varepsilon^2(\log\varepsilon)^2).$$

Inductively,

$$a_{n+1}^* = a_n^* + O(\varepsilon^2(\log\varepsilon)^2)$$

for all $n = O(1)$ with respect to ε. □

When a becomes $\gg O(\varepsilon^2(\log\varepsilon)^2)$, n cannot be $O(1)$ with respect to ε. We now formulate a theorem that is valid for these values a_n^* also:

Theorem 5.3 *The bifurcation values a_n^* satisfy the iterative process*

$$a_{n+1}^* = a_n^* + O(a_n^*).$$

Proof: Let $a = a_n^*$ with $O(1) > a_n^* \gg \varepsilon^2(\log\varepsilon)^2$. Define $p_n = (z_n, k_n)$ by $p_n = P(\Gamma) \cap P^{-n}(\Gamma)$ (the unique intersection point) and take a point $q_n \in P^{-n-1}(\Gamma)$ with z coordinate $z = z_n$. Define $d_n = d(p_n, q_n)$ (see Figure 6). Then $z_n \in (-\sqrt{a_n^*}, \sqrt{a_n^*})$, and thus

$$z_n = O(\sqrt{a_n^*}) \qquad (5.5)$$

Due to the symmetry (at leading order) of $\triangle K(k,z)$ and hence of $P(\Gamma)$ and $P^{-1}(\Gamma)$ around $k=0$, see (2.8)), we find

$$k_n = \frac{1}{2} \triangle K(0,z_n) + \text{h.o.t.} = O(\varepsilon(z_n^2 - a_n^*)) = O(\varepsilon a_n^*) \tag{5.6}$$

by (5.5) since z_n is not too close to $\pm\sqrt{a_n^*}$.

The next step is to determine d_n. We therefore observe that $\mathcal{P}^{-1}(p_n) = (k_n + (\triangle K)^{-1}(k_n,z_n), z_n + (\triangle Z)^{-1}(k_n,z_n))$ and $\mathcal{P}(q_n) = (k_n + \triangle K(k_n,z_n), z_n + \triangle Z(k_n,z_n))$. Since $\triangle Z(k,z) = -\varepsilon \log|k| + 6\varepsilon b + \text{h.o.t.}$, when $|k| \ll 1$ (2.9) and $k_n = O(\varepsilon a_n^*)$, we have $\triangle Z(k_n,z_n) = O(|\varepsilon \log \varepsilon|)$ and the z coordinates of $\mathcal{P}^{-1}(p_n)$ and $\mathcal{P}(q_n)$ are still $O(\sqrt{a_n^*})$. Furthermore, $(\triangle K)^{-1}(k_n,z_n) = O(\varepsilon a_n^*)$ and $\triangle K(k_n,z_n) = O(\varepsilon a_n^*)$ as long as z_n only changes with an $O(|\varepsilon \log \varepsilon|)$ amount.

In other words, both q_n and $\mathcal{P}^{-1}(p_n)$ are mapped over an $O(\varepsilon a_n^*)$ distance with respect to k by $\mathcal{P}$. As a result, $d_n = O(\varepsilon a_n^*)$.

Since $d_n = O(\triangle K(k_{n+1}, z_n, a_{n+1}^*) - \triangle K(k_n, z_n, a_n^*)) = O(\varepsilon(a_{n+1}^* - a_n^*))$, the difference $a_{n+1}^* - a_n^*$ is given by $a_{n+1}^* - a_n^* = O(\frac{d_n}{\varepsilon}) = O(a_n^*)$, and thus

$$a_{n+1}^* = a_n^* + O(a_n^*). \qquad \square$$

Theorem 5.3 implies that a_n^* grows exponentially with n. Hence, if $a_n^* = O(1)$, $a_{n+2}^* \sim a_2^* \cdot \alpha^n = O(1)$ for some α. Thus $n = O(|\log \frac{1}{a_2^*}|) = O(|\log \frac{1}{\varepsilon}|) = O(|\log \varepsilon|)$, since $a_2^* - a^* = O(\varepsilon^2(\log\varepsilon)^2)$ and $a^* = O(\varepsilon)$. In other words: the number N of homoclinic orbits created as a has become $O(1)$ is $O(|\log\varepsilon|)$. This concludes the proof of Theorem 4.2. $\square$

Remark 5.4 In section 4.2 we gave global structures of $W^{\mathrm{u}}(\Gamma)$ and $W^{\mathrm{s}}(\Gamma)$. Therefore we stated that the distance between successive branches was big enough to assume that the slow manifold has hardly any influence on a branch P^{-n-1} when $P^{-n}(\Gamma)$ is tangent to $P(\Gamma)$. Here we proved that this distance is $O(\varepsilon^3(\log\varepsilon)^2)$ (and even bigger for large n). Hence, the influence is topologically negligible indeed, since the slow manifold is important only for points exponentially close to $W^{\mathrm{u}}(\Gamma)$ when one applies $\mathcal{P}^{-1}$.

6 Geometrical analysis of the counteracting case

In this section we fix a at a positive $O(1)$ value (as in Figures 2 and 3). We take this configuration as starting point for the bifurcation analysis for decreasing b. We will use the same techniques as in the cooperating case, but since the structure is more complicated, we mainly do this by examples in section 6.2. Then theorems will be formulated in section 6.3.

Since we have to deal with a very complex structure of $W^{\mathrm{u}}(\Gamma)$ and $W^{\mathrm{s}}(\Gamma)$ in this case, we recall the definitions of some important objects here (see section 4, Figures 3 and 7):

1. A *tongue* $P^n(\Gamma)$ is image under $\mathcal{P}^{n-1}$ of the part of $P(\Gamma)$ with $z_-^* < z < z_+^*$. Similarly, a tongue $P^{-n}(\Gamma)$ is preimage under $\mathcal{P}^{-n+1}$ of the part of $P^{-1}(\Gamma)$ with $z < z_-^*$. We will refer to these tongues as the *first* tongues.

2. Along $P^{-1}(\Gamma)$ an exponentially thin (for $z < z_-^*$) band of *branches* $P^{-n}(\Gamma)$ exists. These are preimages of the part of $P^{-1}(\Gamma)$ with $z > z_+^*$.

3. The preimages of the branches along $P^{-1}(\Gamma)$ form tongues *around* and exponentially close to the first tongues $P^{-n}(\Gamma)$.

Due to intersections of tongues $P^m(\Gamma)$ and $P^{-n}(\Gamma)$ new parts of $W^{\mathrm{u}}(\Gamma)$ and $W^{\mathrm{s}}(\Gamma)$ exponentially close to $P(\Gamma)$ respectively $P^{-1}(\Gamma)$ arise, and their (pre)images will form new tongues around the tongues mentioned in 1 and 3. These new parts emerge as small 'short' tongues, and will eventually become 'infinitely long'.

When the fast flow counteracts the flow on the slow manifold Γ, the structure of $W^{\mathrm{u}}(\Gamma) \cap \{y = 0, x > 1\}$ and $W^{\mathrm{s}}(\Gamma) \cap \{y = 0, x > 1\}$ can be derived using arguments similar to those in section 4.1. The difference is, that $\mathcal{P}$ no longer certainly maps upwards with respect to the z coordinate (and $\mathcal{P}^{-1}$ downwards). This means, that the tongues in $W^{\mathrm{u}}(\Gamma)$ and $W^{\mathrm{s}}(\Gamma)$ are no longer strictly separated by the plane $\{z = z_-^*\}$. However, the global structure of the (first) tongues $P^n(\Gamma)$ and $P^{-m}(\Gamma)$ remains the same. Therefore all intersections in the neighbourhoods of $\gamma^+_{\mathrm{int}}(0)$ and $\gamma^-_{\mathrm{int}}(0)$ also remain (see Figure 3).

We formulate a theorem very similar to Theorem 4.2 for the counteracting case:

Theorem 6.1 *When $a > 0$, $a = O(1)$, and $b \leq -1$, there are at least* two *N-pulse homoclinic orbits for all $N \leq O(|\log \varepsilon|)$. For each such N, one of the N-pulse orbits has all its N fast excursions near the $\{z = z_+^*\}$-plane and the other one makes its first excursion near the plane $\{z = z_-^*\}$ and all other $(N-1)$ excursions near the $\{z = z_+^*\}$-plane.*

Proof: Analogous to the proof of Theorem 4.2. □

The homoclinic orbits mentioned in this theorem are still created by the same mechanism as in the cooperating case when a is varied for some $b \leq -1$ fixed.

6.1 Creating more intersections of $W^{\mathrm{u}}(\Gamma)$ and $W^{\mathrm{s}}(\Gamma)$

When $a > 0$, $a = O(1)$, the global structure of $W^{\mathrm{u}}(\Gamma)$ and $W^{\mathrm{s}}(\Gamma)$ in the counteracting case can be described analogous to the cooperating case as mentioned above. However, now there may be new intersections of the tongues in $W^{\mathrm{u}}(\Gamma)$ and $W^{\mathrm{s}}(\Gamma)$ caused by the counteracting slow and fast fields.

For $b \geq -1$ surely no intersections of tongues $P^{-n}(\Gamma)$ and $P^m(\Gamma)$ exist (see Remark 4.4). For $b < -1$ with $|b| = O(1)$ tongues of $W^{\mathrm{u}}(\Gamma)$, in the neighbourhood of $\{x = 1, y = 0\}$, are mapped upwards with respect to z by $\mathcal{P}^{-1}$, while tongues $W^{\mathrm{s}}(\Gamma)$ in the same neighbourhood are mapped downwards by $\mathcal{P}$. Hence, tongues 'far away' from $P(\Gamma)$ and $P^{-1}(\Gamma)$ may intersect. Recall also from section 2.2, that $\triangle Z(k, z)|_{\{0<k<1\}} > 0$ will only be satisfied for $|b| = O(-\log \varepsilon)$, $b < 0$. Therefore, only then *all* tongues are mapped upwards by $\mathcal{P}$, respectively downwards by $\mathcal{P}^{-1}$.

Of course it is most natural to consider $|b| = O(1)$, but it is much more convenient to consider tongues in the neighbourhood of $P(\Gamma)$ and $P^{-1}(\Gamma)$ than of tongues 'far away'. Therefore, we first assume that $|b| = O(-\log \varepsilon)$ and study the intersecting mechanisms. We will find that these are essentially the same as the mechanisms for tongues in the neighbourhood of $\{x = 1, y = 0\}$, i.e. the tongues 'far away'.

Each pair of first tongues $P^{-n}(\Gamma)$ and $P^m(\Gamma)$ will finally intersect in four points, after a number of bifurcations, when b is negative enough. For further convenience we introduce the following definitions:
We define b_n^i by the value of b for which the *first* tongues $P^n(\Gamma)$ and $P^{-n}(\Gamma)$ are tangent for the first time (see Figure 7). By b_n^{ii} we define the value of b for which the third and fourth intersections of these two tongues are created; in a generic case, $P^n(\Gamma)$ and $P^{-n}(\Gamma)$ are tangent again, see also Figure 9(c). In the same way, $b = b_{n,n+1}^i$, $b = b_{n,n+1}^{ii}$ define values for which the first tongues $P^n(\Gamma)$ and $P^{-n+1}(\Gamma)$ are tangent.

Note, by applying $\mathcal{P}$, $\mathcal{P}^{-1}$ repeatedly, that every intersection of $P^n(\Gamma)$ and $P^{-n}(\Gamma)$ implies that there are also intersections $P^{n+k}(\Gamma)$ and $P^{-n+k}(\Gamma)$ for all $-n < k < n$. In other words, $b_n^{i,ii} = b_{n-k,n+k}^{i,ii}$ for $-n < k < n$.

Note that each 'new' intersection of $P^n(\Gamma)$ and $P^{-m}(\Gamma)$ again corresponds to a homoclinic saddle-node bifurcation. A pair of $(n+m-1)$-pulse homoclinic orbits exists after the initial tangent intersection.

Remark 6.2 In this paper we only consider values of $n \leq O(|\log \varepsilon|)$: so far we have only proved the existence of the tongues $P^{\pm}(\Gamma)$ and of n-pulse homoclinic orbits for $n \leq O(|\log \varepsilon|)$ (Theorems 4.2 and 6.1). In [4] we will find that $n \to \infty$ in the counteracting case.

6.2 Creating new intersections; examples

Before we will formulate general theorems on bifurcations which occur when b is varied, we consider an example of the intersections of tongues and their implications. First, we study the case in which the first tongues $P^3(\Gamma)$ and $P^{-3}(\Gamma)$ intersect in exactly one point, i.e. $b = b_3^i$, to show the correspondence between intersections of different tongues. This correspondence is less clear for the case $b = b_2^i$, however, we will study this case further for next bifurcations since it is less complicated to describe (geometrically).

Figure 7 shows the structure of the intersections of $W^{\mathrm{u}}(\Gamma)$ and $W^{\mathrm{s}}(\Gamma)$ for $b = b_3^i$. All tongues and branches $P^{\pm n}(\Gamma)$ with $n > 4$ are omitted in this figure.

As mentioned above, the tangent intersection $P^3(\Gamma) \cap P^{-3}(\Gamma)$ is mapped by $\mathcal{P}$ and $\mathcal{P}^{-1}$ to tangent intersections $P^k(\Gamma) \cap P^{-6+k}(\Gamma)$, $k = 1, 2, 4, 5$. All these intersections points correspond to one and the same 5-pulse homoclinic orbit. Note that this orbit does not exist in the cooperating case.

Like in the cooperating case, $P^{-2}(\Gamma)$ consists of two disjoint parts, $P^{-3}(\Gamma)$ of three and $P^{-4}(\Gamma)$ of four parts as shown in Figure 7. Also $P^{-5}(\Gamma)$ consists of five disjoint parts, but $P^{-k}(\Gamma)$, $k > 5$ contain new parts inside the domain of $\mathcal{P}^{-1}$ besides the k parts we already encountered in the cooperating case. We will describe $P^{\pm 5}(\Gamma)$ and $P^{\pm 6}(\Gamma)$ to explain this.

When $b = b_3^i$, the first tongue $P^5(\Gamma)$ intersects $P^{-1}(\Gamma)$ in exactly one point, and $P^{-5}(\Gamma)$ 'touches' $P(\Gamma)$, corresponding with the intersection $P^3(\Gamma) \cap P^{-3}(\Gamma)$. But since $P^5(\Gamma)$ intersects $P^{-1}(\Gamma)$, it contains points exponentially close to $P^{-1}(\Gamma)$. Hence, by Lemma 3.4, the image $P^6(\Gamma)$ of $P^5(\Gamma)$ contains parts with large positive z coordinate, exponentially close to $P(\Gamma)$. By continuity arguments, $P^6(\Gamma)$ has only one new discontinuity, namely the image of the intersection point $P^5(\Gamma) \cap P^{-1}(\Gamma)$. Hence, the 'tip' of the (first) $P^6(\Gamma)$

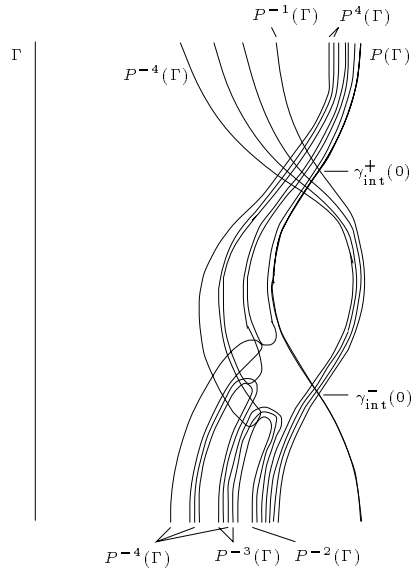

Figure 7: The homoclinic tangency corresponding with $b = b_3^i$. The intersection point $P^3(\Gamma)$ and $P^{-3}(\Gamma)$ corresponds to the same (5-pulse) homoclinic orbit as the points $P^4(\Gamma) \cap P^{-2}(\Gamma)$ and $P^2(\Gamma) \cap P^{-4}(\Gamma)$.

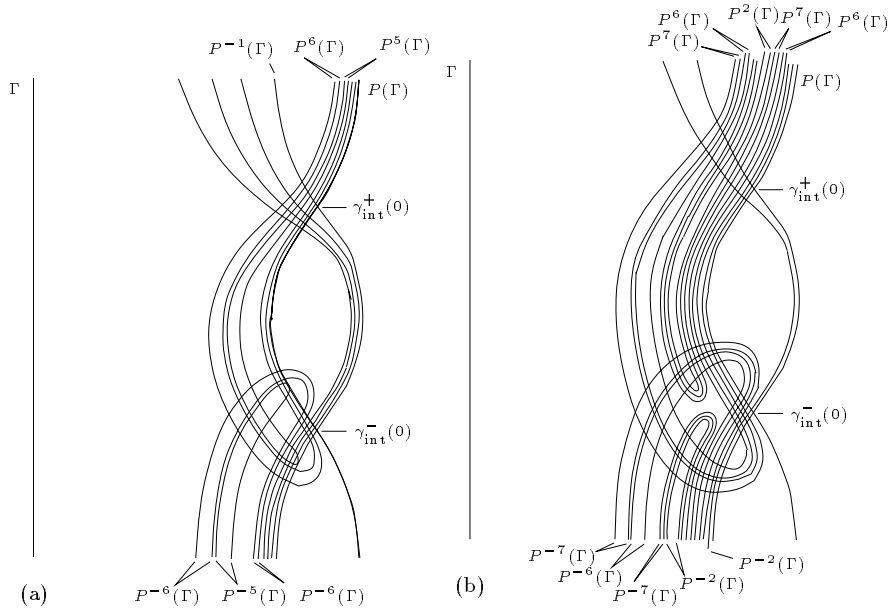

Figure 8: Folding of the first tongues $P^6(\Gamma)$ and $P^{-6}(\Gamma)$ for $b = b_3^i$ (a) and their (pre)images (b). All first tongues $P^{\pm n}(\Gamma)$ with $n = 2, 3, 4$ (and $n = 5$ for (b)) are omitted.

tongue has now been mapped to $+\infty$: the $P^6(\Gamma)$ tongue has been folded towards $P(\Gamma)$ – the distance is of course exponentially small, see Figure 8(a).

Since $P^5(\Gamma)$ and $P^6(\Gamma)$ are disjoint (otherwise there should be a fixed point of $\mathcal{P}$) $P^6(\Gamma)$ contains parts outside $P^{-1}(\Gamma)$, so outside the domain on which $\mathcal{P}$ is defined. But it also contains two 'new' branches exponentially close to $P(\Gamma)$, so what used to be one tongue in the cooperating case has been cut into four parts in the domain in which $\mathcal{P}$ is defined. The images of these four parts are four disjoint subsets of $P^7(\Gamma)$, again all 'folded towards' $P(\Gamma)$ since the four parts $P^6(\Gamma)$ all intersect $P^{-1}(\Gamma)$. See Figure 8(b).

Similar arguments show that $P^{-6}(\Gamma)$ folds towards $P^{-1}(\Gamma)$, etc. Note, that all arguments are also applicable for the higher order tongues around $P^{-6}(\Gamma)$ and other first tongues $P^{-n}(\Gamma)$, $n > 6$.

6.2.1 Intersections of tongues and their implications

We already observed, that tongues $P^6(\Gamma)$ and $P^{-6}(\Gamma)$ are folded towards $P(\Gamma)$ respectively $P^{-1}(\Gamma)$ when $P^3(\Gamma)$ and $P^{-3}(\Gamma)$ are tangent. In general, when $b = b_n^i$, the same mechanism as described in section 6.2 causes the tongues $P^{2n}(\Gamma)$ and $P^{-2n}(\Gamma)$ to be folded towards $P(\Gamma)$ respectively $P^{-1}(\Gamma)$.

In this subsection we will study the process leading to 'folded tongues', and determine where the images, respectively preimages, of the new parts of $P^{2n}(\Gamma)$ and $P^{-2n}(\Gamma)$ are situated. Again new intersection points corresponding with new homoclinic orbits will appear.

The different stages for values of b between $b = b_2^i$ and $b = b_{2,1}^i$ are relatively easy to describe and are representative for bifurcations between the more general bifurcations at $b = b_n^i$ and $b = b_{n,n-1}^i$, so we will start with b slightly larger than b_2^i and follow the bifurcations for decreasing b. Figure 9 shows the structure of $W^{u,s}(\Gamma) \cap \{y = 0, x > 1\}$ for different values of b between b_2^i and $b_{1,2}^i$; Figures 9(a)-(c)are restricted to a neighbourhood of the $\{z = z_-^*\}$ plane. Only parts $P^{\pm k}(\Gamma)$ with $k \leq 3$ of $W^u(\Gamma) \cap \{y = 0, x > 1\}$ and $W^s(\Gamma) \cap \{y = 0, x > 1\}$ are taken into account, unless this does not satisfactory explain the behaviour.

For $b = b_2^i$, the first tongues $P^2(\Gamma)$ and $P^{-2}(\Gamma)$ are tangent, and so are $P^3(\Gamma)$ and $P^{-1}(\Gamma)$, and $P^{-3}(\Gamma)$ and $P^1(\Gamma)$. This implies for the exponentially thin bands along $P^{-1}(\Gamma)$ and around the first tongues $P^{-2}(\Gamma)$ and $P^{-3}(\Gamma)$, that every branch or tongue in them has already two intersection points with $P^3(\Gamma)$, $P^2(\Gamma)$ respectively $P(\Gamma)$. Just before b reached the value $b = b_2^i$, these branches were tangent to $P^2(\Gamma)$ one after another. Thus, we note that there must have been $\gg 1$ bifurcations for b larger than, but exponentially close to b_2^i. In Figure 9(a) $P^{-3}(\Gamma)$ (which lies around $P^{-2}(\Gamma)$) and $P^2(\Gamma)$ are tangent.

In Figure 9(b) we consider the case in which the 'tip' of the $P^{-2}(\Gamma)$ tongue enters the $P^2(\Gamma)$ tongue. In section 6.4 we shall distinguish between the three different situations which can follow after the first intersection of these two tongues ($P^{-2}(\Gamma)$ can enter $P^2(\Gamma)$, $P^2(\Gamma)$ can enter $P^{-2}(\Gamma)$ and the transition between these). The next new intersections occurs as $P^{-2}(\Gamma)$ becomes again tangent to $P^2(\Gamma)$ for $b = b_2^{ii}$, now 'from the inside', see Figure 9(c). This new intersection is mapped by $\mathcal{P}$ and $\mathcal{P}^{-1}$ to intersections $P^3(\Gamma) \cap P^{-1}(\Gamma)$ and $P^{-3}(\Gamma) \cap P(\Gamma)$: both first tongues $P^{\pm 3}(\Gamma)$ have a part outside the definition domains of

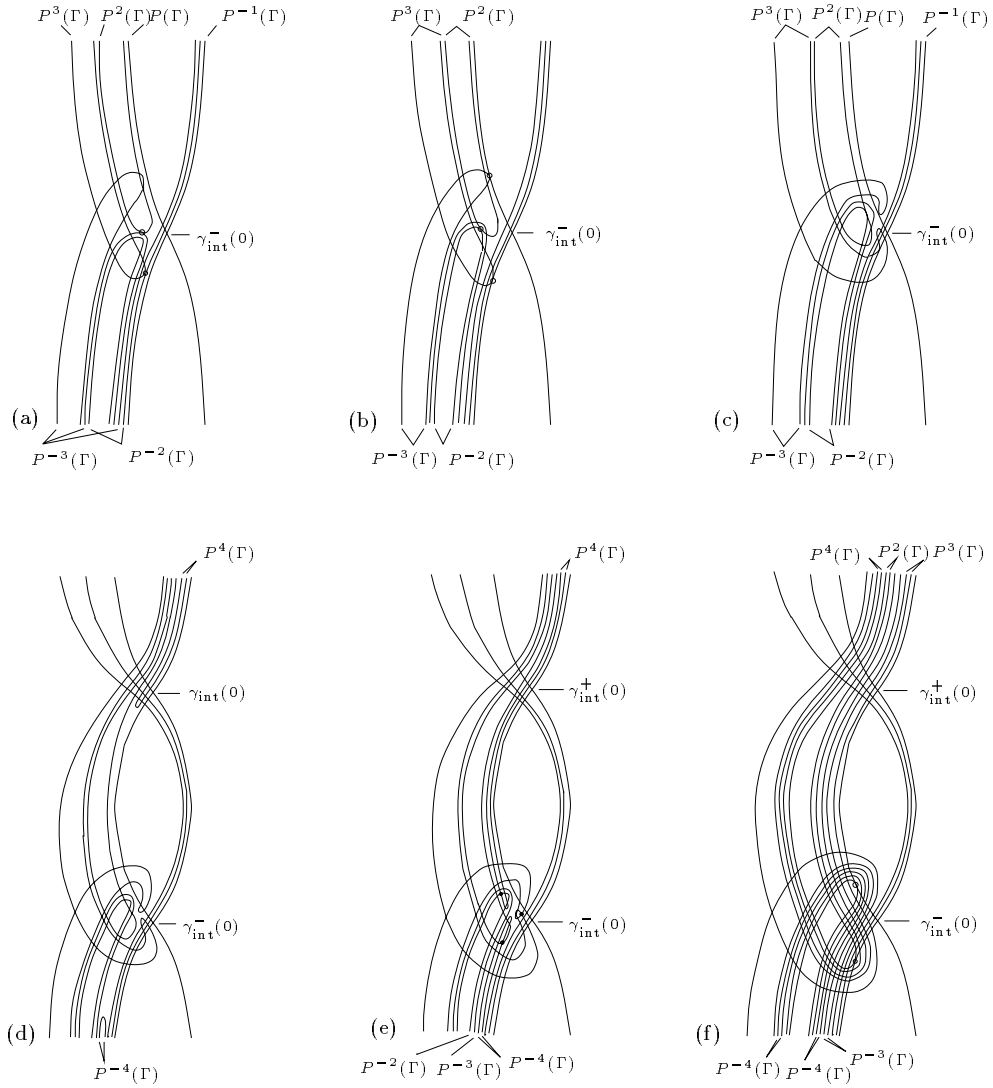

Figure 9: Intersections of $W^{\rm u}(\Gamma)$ and $W^{\rm s}(\Gamma)$ with $\{y = 0, x > 1\}$ for decreasing b between $b = b_2^i$ and $b = b_{1,2}^i$; (b) $b = b_2^i$: tongues $P^{\pm 4}(\Gamma)$ have folded back to $P^{\pm 1}(\Gamma)$; (c) $b = b_2^{ii}$; (f) $b = b_{1,2}^i$.

$\mathcal{P}$ respectively $\mathcal{P}^{-1}$. Note that $P^3(\Gamma)$ and $P^{-3}(\Gamma)$ fold in a different way. The geometrical reason for this is explained in section 6.4.

When the tangency corresponding with $b = b_2^{ii}$ breaks, the first tongues $P^3(\Gamma)$ respectively $P^{-3}(\Gamma)$ again enter the domains in which $\mathcal{P}$ and $\mathcal{P}^{-1}$ are defined. The tongues have folded across $P^{-1}(\Gamma)$ and $P(\Gamma)$, but do not reach $z = \pm\infty$, yet. This is shown in Figure 9(d). The new part $P^3(\Gamma)$ inside $P^{-1}(\Gamma)$ still lies exponentially close to $P^{-1}(\Gamma)$ and hence its image is a thin tongue $P^4(\Gamma)$ exponentially close to $P(\Gamma)$ with large z coordinates (by Lemma 3.4). All intersection points of the tip of $P^3(\Gamma)$ with the branches exponentially close to $P^{-1}(\Gamma)$ in Figure 9(d) are mapped by $\mathcal{P}$ to intersections of the thin tongue $P^4(\Gamma)$ with the first tongues $P^{-n}(\Gamma)$, $n > 1$, near the plane $\{z = z_+^*\}$.

When the tips of tongues $P^3(\Gamma)$ and $P^{-3}(\Gamma)$ intersect each other in the neighbourhood of $\gamma_{\rm int}^-(0)$, the thin tongues $P^4(\Gamma)$ and $P^{-4}(\Gamma)$ intersect the first tongues $P^{-2}(\Gamma)$ respectively $P^2(\Gamma)$ (see Figure 9(e)).

Finally, at $b = b_{1,2}^i$, the first tongues $P^{\pm 2}(\Gamma)$ are tangent to $P^{\mp 1}(\Gamma)$. Hence they contain points exponentially close to $P^{\mp}(\Gamma)$ and their images (respectively preimages) $P^{\pm 3}(\Gamma)$ are now branches which reach $z = \pm\infty$. The largest parts of these branches $P^{\pm 3}(\Gamma)$ no longer lie close to $\gamma_{\rm int}^-(0)$ and thus they are now mapped over an $O(\varepsilon)$ distance by Lemma 3.1. Hence, the small tongues $P^{\pm 4}(\Gamma)$ contain parts $O(\varepsilon)$ away from $P^{\pm}(\Gamma)$ and fold around $P^{\pm 2}(\Gamma)$, back to $z = \pm\infty$.

6.3 Theorems on creating new saddle-node bifurcations

The observations in the previous section lead to several theorems on new homoclinic saddle-node bifurcations. The first is on the tangencies corresponding with b_n^i:

Theorem 6.3 *Assume $a > 0$, $a = O(1)$. Besides the two N-pulse homoclinic orbits, $N \geq 1$, mentioned in theorem 6.1, other homoclinic orbits appear in various saddle-node bifurcations when b decreases from zero. The first bifurcations happen for $b < -1$, $b = O(1)$.*

The first tongues $P^n(\Gamma)$ and $P^{-n}(\Gamma)$ are tangent for $b = b_n^i$. Hence, tongues $P^{n+k}(\Gamma)$ and $P^{-n+k}(\Gamma)$ are tangent, and there exists a $(2n-1)$-pulse homoclinic orbit .

For $b < b_n^i$, two $(2n-1)$-pulse homoclinic orbits have bifurcated from this homoclinic tangency, so each bifurcation b_n^i results in two *new N-pulse homoclinic orbits, where $N = 2n-1$. The bifurcation values form a monotone sequence $b_2^i < b_3^i < b_4^i < \ldots < -1$.*

Proof: It is clear, that each bifurcation b_n^i results in two new $(2n-1)$-pulse homoclinic orbits *if the bifurcation really occurs*. The $2n-1$ pulses correspond with the $2n-1$ times the orbit intersects the plane $\{y = 0, x > 1\}$ (in points $P^k(\Gamma) \cap P^{-l}(\Gamma)$ with $k + l = 2n$, $k, l \geq 1$). We have to show, that *all* bifurcation values are reached when b decreases and that the homoclinic saddle-node bifurcations at $b = b_n^i$ form a monotone sequence.

First note (by (2.8)), that for each $-\frac{1}{6} < k < 0$ fixed

$$\frac{\partial}{\partial b} \triangle Z(k,z) = 2\varepsilon \int_{x_1(k)}^{x_2(k)} \frac{x}{\sqrt{2k + x^2 - \frac{2}{3}x^3}} dx + O(\varepsilon^2).$$

Here $x_1(k)$ and $x_2(k)$ are the (positive) values for which $2k + x^2 - \frac{2}{3}x^3 = 0$. The integral

$$T_1(k) = 2\int_{x_1(k)}^{x_2(k)} \frac{x}{\sqrt{2k + x^2 - \frac{2}{3}x^3}}dx = \oint \frac{x}{\sqrt{2k + x^2 - \frac{2}{3}x^3}}dx$$

is a strictly positive and monotonous function of k. Furthermore, $\lim_{k\to -\frac{1}{6}} T_1(k) = 2\pi$ and $\lim_{k\to 0} T_1(k) = 6$ (see Appendix A of [5]). Hence, $\triangle Z(k,z)$ is a strictly monotone function of b and $\lim_{b\to -\infty} \triangle Z(k,z) = -\infty$ for all $-\frac{1}{6} < k < 0$.

This implies that every pair of tongues will eventually intersect if b becomes negative enough.

The (first) tongues $P^n(\Gamma)$ and $P^{-n}(\Gamma)$ are unbounded in the positive respectively negative z direction and they are ordered from right to left with increasing n. Therefore an intersection of the first tongues $P^n(\Gamma) \cap P^{-n}(\Gamma)$ implies intersections $P^j(\Gamma) \cap P^{-j}(\Gamma)$ for all $j > n$ and hence all bifurcations at values $b = b_j^i$, $j > n$, must have occurred before b reached the value b_n^i if b decreases monotonously. Moreover, since b varies continuously and $\triangle Z$ is monotone in b, intersections $P^n(\Gamma) \cap P^{-n}(\Gamma)$ and $P^{n+1}(\Gamma) \cap P^{-n-1}(\Gamma)$ cannot arise at the same moment. Therefore, the sequence $b_2^i < b_3^i < b_4^i < \ldots < -1$ is a monotone sequence of homoclinic bifurcations. □

As a next step, the bifurcations $b_{n,n+1}^i$ will complete this sequence as formulated in the following theorem.

Theorem 6.4 *Let $a > 0$, $a = O(1)$, and b decreasing from zero. For $b = b_{n,n+1}^i$, two $2n$-pulse homoclinic orbits appear in a saddle-node bifurcation. The values $b = b_{n,n+1}^i$, $n > 1$ satisfy $b_n^i < b_{n,n+1}^i < b_{n+1}^i$, and $b_{1,2}^i < b_2^i$.*

Proof: By the same ordering argument as in the proof of Theorem 6.3, the first tongues $P^n(\Gamma)$ and $P^{-n+1}(\Gamma)$ have four intersection points when the first tongues $P^n(\Gamma)$ and $P^{-n}(\Gamma)$ (and hence $P^{n\pm 1}(\Gamma)$ and $P^{n\mp 1}(\Gamma)$) intersect. Therefore, and since the bifurcation values are distinct as mentioned above, $b_{n,n+1}^i > b_n^i$.

In the same way, intersections of first tongues $P^n(\Gamma) \cap P^{-n-1}(\Gamma)$ and $P^{n+1}(\Gamma) \cap P^{-n}(\Gamma)$ imply that the first tongues $P^{-n-1}(\Gamma)$ and $P^{n+1}(\Gamma)$ intersect each other, and hence the latter tongues already intersect for $b = b_{n,n+1}^i$. Thus, $b_{n,n+1}^i < b_{n+1}^i$. □

Before we will formulate a similar theorem on the bifurcation values b_n^{ii}, $b_{n,n+1}^{ii}$, we will distinguish different ways of intersecting for these bifurcations in the next section.

6.4 Topologically different ways of intersecting

We already mentioned, that intersections $P^n(\Gamma) \cap P^{-m}(\Gamma)$ of the original tongues can be created in different ways. In fact, the creation of the first two intersection points in a tangency is topologically the same in every case, but there are three possibilities for the creation of the third and fourth intersection points. The difference between these three possible ways of creating new intersections is quite delicate and deals with the relative 'velocity' of the tongues. In Figure 10 this difference is shown.

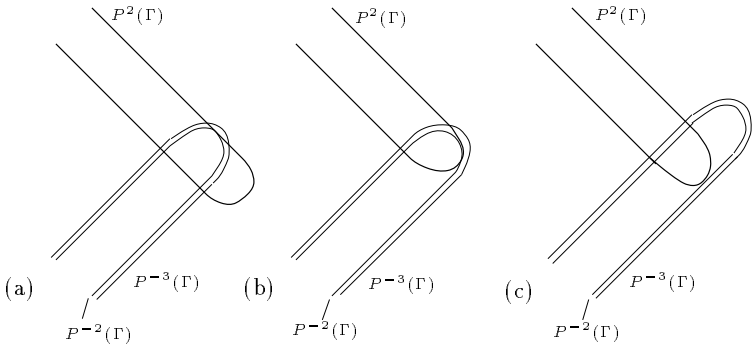

Figure 10: Creation of intersection points in different orders; (a) Case 1, (b) Case 3; (c) Case 2.

Again we take the tongues $P^{\pm 2}(\Gamma)$ as an example. First suppose that $P^2(\Gamma)$ moves faster than $P^{-2}(\Gamma)$ when b decreases. Then the top of $P^{-2}(\Gamma)$ touches a long side of $P^2(\Gamma)$ when $b = b_2^i$, and after a while it touches the other long side of $P^2(\Gamma)$ for $b = b_2^{ii}$ (see Figures 9(b) and (c)). We observe that all branches in the exponentially thin band around $P^{-2}(\Gamma)$ already intersect $P^2(\Gamma)$ in four points. This is Case 1, see Figure 10(a).

In Case 2 $P^2(\Gamma)$ moves slower than $P^{-2}(\Gamma)$ when b decreases. In this case, for $b = b_2^i$ and $b = b_2^{ii}$, the top of $P^2(\Gamma)$ is tangent to a long side of $P^{-2}(\Gamma)$. At $b = b_2^{ii}$, all branches around $P^{-2}(\Gamma)$ still intersect $P^2(\Gamma)$ in only two points (Figure 10(c)).

These slightly different situations appear to be very important for the way the first tongues $P^{\pm 3}(\Gamma)$ fold back. We do not need to understand the necessity of different mechanisms when we only study the behaviour of tongues $P^{-n}(\Gamma)$ without taking into account the exponentially thin bands around them. However, by a careful analysis of the order in which new intersection points (in the exponentially thin bands along $P^{-1}(\Gamma)$ and around $P^{-2}(\Gamma)$) are created we conclude that in Case 1 the tongue $P^3(\Gamma)$ necessarily folds back through $P^{-1}(\Gamma)$ (so it first intersects $P^{-1}(\Gamma)$ in four points before it intersects the branch $P^{-2}(\Gamma)$ four times, etc.), while $P^{-3}(\Gamma)$ creates its intersections with $P(\Gamma)$ by 'indentation' (see Figure 11). In Case 2, however, the tongue $P^3(\Gamma)$ necessarily creates intersections with $P^{-1}(\Gamma)$ by indentation (and thus it first intersects the branch $P^{-2}(\Gamma)$ in four points before it intersects $P^{-1}(\Gamma)$ itself four times), while $P^{-3}(\Gamma)$ folds back through $P(\Gamma)$. (In Figure 9 the $P^{\pm 2}(\Gamma)$ tongues behave as in Case 1.)

In between these two cases, obviously both tongues have the same velocity. In this degenerate case, Case 3, there is no second tangency, but the third and fourth intersection points are created in a third order intersection point (a cubic homoclinic tangency), see Figure 10(b). At this moment the branches around $P^{-2}(\Gamma)$ still intersect $P^2(\Gamma)$ in only two points. The other intersections of these branches with $P^2(\Gamma)$ are created in the same order as in Case 2.

Remark 6.5 In [11] Holmes and Whitley encountered the same topologically different ways of intersections of stable and unstable manifolds when they studied homoclinic bifurcations of two-dimensional maps.

We do not have any quantitative method to decide which of the cases occurs in our

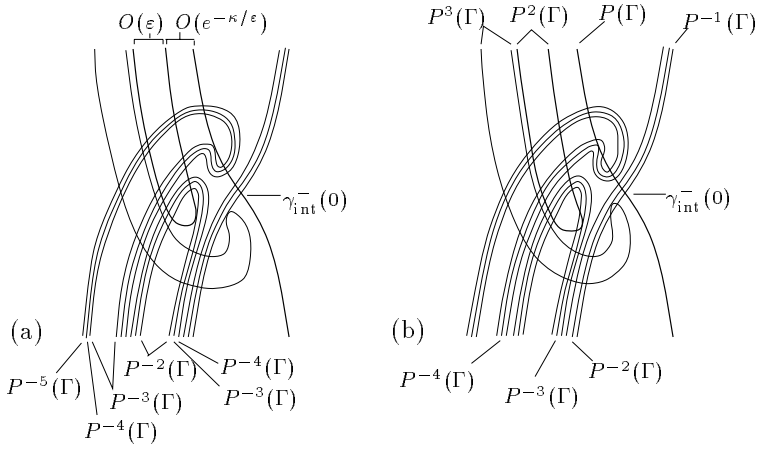

Figure 11: The indentation of $P^{-3}(\Gamma)$ and branches around this tongue, and the folding back of $P^3(\Gamma)$; (a) $P^{-2}(\Gamma)$ and $P^2(\Gamma)$ are tangent, (b) b is a little more negative: $P^2(\Gamma)$ is tangent to the branch $P^{-3}(\Gamma)$.

model systems (1.1) and (2.3). However, independent of the mechanism of intersecting, we can formulate the following theorem.

Theorem 6.6 *Let $a > 0$, $a = O(1)$, and b decreasing from zero. Then, for $b = b_n^{ii}$ (respectively $b = b_{n,n+1}^{ii}$), a third, tangent, intersection of the first tongues $P^n(\Gamma)$ and $P^{-n}(\Gamma)$ (respectively $P^{-n-1}(\Gamma)$ exists. If this is not the case, then one of the two transversal intersection points $P^n(\Gamma) \cap P^{-n}(\Gamma)$ which already exist has become a third order intersection point.*

For $b < b_n^{ii}$ (respectively $b < b_{n,n+1}^{ii}$) two $2n-1$ (respectively $2n$)-pulse homoclinic orbits have bifurcated from the tangent intersection, or three such orbits have bifurcated from the third order intersection.

The values $b = b_n^{ii}$ and $b = b_{n,n+1}^{ii}$ satisfy $b_{n-1,n}^{i} < b_n^{ii} < b_n^{i} < b_{n,n+1}^{ii} < b_{n,n+1}^{i}$ for all $n > 1$.

Proof: We only have to proof the ordering stated in this theorem, since the rest follows from earlier proofs. Obviously, $b_n^{ii} < b_n^i$ and $b_{n,n+1}^{ii} < b_{n,n+1}^i$. Again by the ordering of the tongues, the first tongues $P^n(\Gamma)$ and $P^{-n}(\Gamma)$ cannot intersect when the first tongues $P^n(\Gamma)$ and $P^{-n-1}(\Gamma)$ are tangent. Hence $b_n^i < b_{n,n+1}^{ii}$ for all $n > 1$, and in the same way we obtain $b_{n-1,n}^i < b_n^{ii}$. □

Thus far, we have a sequence $b_{1,2}^i < b_2^{ii} < b_2^i < b_{2,3}^{ii} < b_{2,3}^i < \ldots < -1$ of bifurcations, where each bifurcation results in two new homoclinic orbits. This leads to the following amounts of N-pulse orbits:

Theorem 6.7 *When $a = O(1)$, $b = O(-\log \varepsilon) < 0$ (b is negative enough), there exist six N-pulse homoclinic orbits for each $N \geq 3$, that are created in bifurcations a_i^* and $b_n^{i,ii}$, $b_{n,n+1}^{i,ii}$. Since the sequence of bifurcations ends with $b_{1,2}^i$, there are only four 2-pulse orbits.*

Note that we so far did not take into account the 'higher order' branches exponentially close to $P^{-1}(\Gamma)$ below $z \sim z_-^*$. The preimages of these branches are 'higher order' tongues

that are folded exponentially close around the first tongues $P^{-n}(\Gamma)$ like in the cooperating case, and of course intersections of a first tongue $P^{-n}(\Gamma)$ will imply intersections of the tongues around it. These intersections also appear in homoclinic saddle-node bifurcations, just before b (which is still decreasing) reaches a value $b_{k,l}^{i,ii}$: for $k+l = N+1 \geq 3$ two N-pulse homoclinic orbits are created, and a sequence of $(N+M)$-pulse orbits, two for each $M > 0$, has arisen short before $b = b_{k,l}^{i,ii}$ (or arises short after $b = b_{k,l}^{i,ii}$ in Case 2 – Figure 10(c)).

For b negative enough these bifurcations lead to $4(N-2)-2$ more N-pulse homoclinic orbits for each $N > 2$. Note that $P^{-2}(\Gamma)$ is the first branch along $P^{-1}(\Gamma)$, and hence all homoclinic orbits created in these bifurcations have at least three (corresponding to $P^2(\Gamma) \cap P^{-2}(\Gamma)$) pulses through the fast field.

These observations can be formulated in the following theorem:

Theorem 6.8 *Exponentially close to b^i and b^{ii} there exist additional homoclinic saddle-node bifurcations. As a consequence, there are at least $4(N-1)$ N-pulse homoclinic orbits for $N > 2$ when $a = O(1)$, $b = O(-\log\varepsilon) < 0$; there are still two 1-pulse homoclinic orbits.*

Although we already concluded that the sequence above is not complete at all, we still only mentioned the intersections of what used to be a tongue in the cooperating case. In paragraph 6.2.1 we saw that a new 2-pulse homoclinic orbit implies the appearance of new small tongues and many new intersections (see Figure 9(f)). The same can be concluded for other values of n:

Every intersection $P^n(\Gamma) \cap P^{-n}(\Gamma)$ implies the two intersections $P^{2n-1}(\Gamma) \cap P^{-1}(\Gamma)$ and $P^{-2n+1}(\Gamma) \cap P(\Gamma)$ as follows. We focus on the point $P^{2n-1}(\Gamma) \cap P^{-1}(\Gamma)$, which exists since we have an intersection $P^n(\Gamma) \cap P^{-n}(\Gamma)$. The Poincaré map $\mathcal{P}$ is well defined for points on $P^{2n-1}(\Gamma)$ below this intersection point. Hence, $P^{2n-1}(\Gamma)$ contains points, on which $\mathcal{P}$ works, arbitrarily close to a $2n-1$-pulse homoclinic orbit. By Lemma 3.4 these points have images exponentially close to $P^{-1}(\Gamma)$, hence the tongue $\mathcal{P}(P^{2n-1}(\Gamma)) = P^{2n}(\Gamma)$ folds towards $P^{-1}(\Gamma)$. By applying the map $\mathcal{P}^{-1}$ on $P^{-2n+1}(\Gamma)$ we can conclude the same for the tongue $P^{-2n}(\Gamma)$. In Figure 9(b) these observations are outlined for $n = 2$.

Thus, if $b = b_n^*$ (or $b < b_n^*$) the intersections $P^{2n}(\Gamma)$ and $P^{-2n}(\Gamma)$ of $W^{\mathrm{u}}(\Gamma)$ and $W^{\mathrm{s}}(\Gamma)$ with the plane $\{y = 0, x > 1\}$ contain a new part inside the definition area of $\mathcal{P}$ and $\mathcal{P}^{-1}$. This part of $P^{2n}(\Gamma)$ consists of two branches, stretching out from points which lie below $\gamma_{\mathrm{int}}^-(0)$ to $z = \infty$. In the same way, the new part of $P^{-2n}(\Gamma)$ stretches out from points which lie above $\gamma_{\mathrm{int}}^-(0)$ to $z = -\infty$. This implies four intersection points $P^{2n}(\Gamma) \cap P^{-2n}(\Gamma)$, close to the point $\gamma_{\mathrm{int}}^-(0)$. Applying $\mathcal{P}$ and $\mathcal{P}^{-1}$ on these intersections $2n-1$ times, one obtains intersections $P^{4n-1}(\Gamma) \cap P^{-1}(\Gamma)$ and $P^{-4n+1}(\Gamma) \cap P(\Gamma)$ and thus the next image respectively preimage again fold towards and contain parts exponentially close to $P(\Gamma)$ respectively $P^{-1}(\Gamma)$. By the same argument the tongues $P^{4n}(\Gamma)$ and $P^{-4n}(\Gamma)$ intersect in a neighbourhood of $\gamma_{\mathrm{int}}^-(0)$ and repeatedly applying $\mathcal{P}$ and $\mathcal{P}^{-1}$ on their intersection points we can conclude the same for $P^{2^k n}(\Gamma)$ and $P^{-2^k n}(\Gamma)$ for $k > 2$.

All bifurcations corresponding with the creation of these intersections and homoclinic orbits through these intersection points are not included in the sequence of $b_n^{i,ii}$ and $b_{n,n+1}^{i,ii}$ either. We now state a theorem on intersections which are created by the tongues which are folded towards $P(\Gamma)$ and $P^{-1}(\Gamma)$. This theorem is based on observations in section 6.2.1.

Theorem 6.9 *For $b_n^{ii} > b > b_{n-1,n}^{i}$, the first tongues $P^{2n-1}(\Gamma)$ and $P^{-2n+1}(\Gamma)$ consist of three disjoint parts in the domains of $\mathcal{P}$, respectively $\mathcal{P}^{-1}$. A small 'new' tongue $P^{2n-1}(\Gamma)$ is growing upwards from $P^{-1}(\Gamma)$, exponentially close to $P(\Gamma)$, for decreasing b, and intersections with all first tongues P^{-k}, $k \geq 2n-2$, appear one after another, until the small tongue reaches $z = \infty$ for $b = b_{n,n-1}^{i}$. At the same time, a small tongue $P^{-2n+1}(\Gamma)$ is growing downwards from $P(\Gamma)$ and intersections with all tongues $P^{k}(\Gamma)$, $k \geq 2n-2$, appear. All these new intersections correspond with new homoclinic orbits.*

Remark 6.10 We can conclude from this mechanism that all new images and preimages which lie exponentially close to $P(\Gamma)$ respectively $P^{-1}(\Gamma)$ will again cause many new intersection points, so there are many homoclinic bifurcations besides the ones we already encountered.

Moreover, one must realize that all bifurcations happen very close after each other. For example, consider Figures 9(c) to (f): the original tongue $P^{-2}(\Gamma)$ moved upwards, but this movement was only exponentially small. In between many homoclinic tangencies arose. This seems to be reminiscent to a result of Newhouse's work ([17]): the homoclinic tangencies are persistent in the sense that if we destroy a particular tangency we will create another elsewhere.

7 Discussion

The second parameter b plays an extremely important role in the analysis of the a priori rather simple model problem (1.1). Since we did not derive the model problem from a general system (1.5) by some kind of reduction and/or unfolding method, it is not immediately clear whether the equivalent of b exists naturally in systems like (1.5). On the other hand, it is quite clear from (1.5) that the direction of the flow along a slow (normally hyperbolic manifold) is controlled by an expression in F, g_1 and g_2 that differs essentially from the expression that determines the sign of $\triangle Z$. It is shown in [2] that these two quantities are completely independent in the case of (1.5) for a Ginzburg-Landau equation with a small quintic term.

The essential difference between the cooperating ($b > -1$) and the counteracting case is that the $P^{n}(\Gamma)$ tongues cannot intersect the $P^{-m}(\Gamma)$ tongues in the cooperating case. As b decreases through -1 some tongues start to intersect and create many new families of homoclinic orbits. In [5], [2] two different types of homoclinic explosions and implosions are described. The difference between these cases is exactly the same as between the cooperating and the counteracting case: in the most simple case it is shown that the $P^{n}(\Gamma)$ and $P^{-m}(\Gamma)$ tongues cannot intersect before the explosion (or after the implosion) at a critical value ν^* of a certain parameter ν. In the other case the tongues do intersect before (explosion) or after (implosion) $\nu = \nu^*$, therefore, the global bifurcation then appears at a $O(|\log \varepsilon|)$ ([2]) distance from ν^* and is much more complicated than in the other 'cooperating' case. Both in [5] and [2] it is remarked that the 'counteracting' case is not at all fully understood. Since the existence of critical points on Γ in [5] and [2] makes the structure of $W^{\mathrm{s}}(\Gamma)$ and $W^{\mathrm{u}}(\Gamma)$ more complex, we have been able in section 6 to understand more of the consequences of the intersection of the $P^{n}(\Gamma)$ and $P^{-m}(\Gamma)$ tongues than in [5] and [2].

Finally, we remark that, in this paper, we focused on the creation of orbits biasymptotic to the slow manifold Γ of (1.1) (or, in case of model problem (2.3): heteroclinic orbits between the critical points S^+ and S^- on Γ). We described the structure of the manifolds $W^s(\Gamma)$ and $W^u(\Gamma)$ by analysing the intersections of $W^s(\Gamma)$ and $W^u(\Gamma)$ with the half-plane $\{y = 0, x > 1\}$. However, in section 6 we found that the (pre-)images $P^n(\Gamma)$ and $P^{-m}(\Gamma)$ became less and less suited to give a clear description of $W^s(\Gamma) \cap W^u(\Gamma)$. In order to obtain a better understanding of $W^s(\Gamma) \cap W^u(\Gamma)$ in the counteracting case, we first need to develop a better 'tool' . This will be the subject of future work ([4]). Here, other, non-homoclinic solutions to (1.1) will also be considered. In particular, under suitable assumptions, we can show that the Poincaré map $\mathcal{P}^{-1}$ contains a subshift of finite type. In doing so, we obtain more insight in the structure of $W^s(\Gamma) \cap W^u(\Gamma) \cap \{y = 0, x > 1\}$ by interpreting its structure in terms of the symbolic dynamics associated to the subshift.

Acknowledgement The authors thank Philip Holmes for stimulating discussions.

References

[1] R. Camassa, G. Kovačič, and S.-K. Tin. A Melnikov method for homoclinic orbits with many pulses. *to appear in Arch. Rat. Mech. Anal.*, 1996.

[2] A. Doelman. Breaking the hidden symmetry in the Ginzburg-Landau equation. *Physica D*, **97**:398–428, 1996.

[3] A. Doelman and W. Eckhaus. Periodic and quasi-periodic solutions of degenerate modulation equations. *Physica D*, **53**:249–266, 1991.

[4] A. Doelman, G. Hek, P. Holmes, and E. Lynch. In preparation.

[5] A. Doelman and P. Holmes. Homoclinic explosions and implosions. *Phil. Trans. R. Soc. Lond. A* , **354**:845–893, 1995.

[6] J. Duan and P. Holmes. Fronts, domain walls and pulses for a generalized Ginzburg-Landau equation. *Proc. Edinburgh Math. Soc.*, **38**:77–97, 1994.

[7] W. Eckhaus. On modulation equations of the Ginzburg-Landau type. In R.E. O'Malley, editor, *ICIAM 91: Proc. 2nd Int. Conf. Ind. Appl. Math.*, pages 83–98, 1992.

[8] N. Fenichel. Geometric singular perturbation theory for ordinary differential equations. *J. Diff. Eq.*, **31**:53–98, 1979.

[9] J. Guckenheimer and P.J. Holmes. *Nonlinear oscillations, Dynamical systems and Bifurcations of Vector Fields* . Springer Verlag New York etc., 1983.

[10] P. Holmes. Spatial structure of time-periodic solutions of the Ginzburg-Landau equation. *Physica D*, **23**:84–90, 1986.

[11] P. Holmes and D. Whitley. Bifurcations of one- and two-dimensional maps. *Phil. Trans. R. Soc. Lond. A* , **311**:43–102, 1984.

[12] C.K.R.T. Jones. Geometric Singular Perturbation Theory. In R. Johnson, editor, *Dynamical Systems, Montecatibi Terme, L.N.M.*, volume **1609**. Springer-Verlag New York etc., 1994.

[13] C.K.R.T. Jones, T.J. Kaper, and N. Kopell. Tracking Invariant Manifolds up to Exponentially Small Errors. *SIAM J. Math. Anal.*, **27**(2):558–577, 1996.

[14] C.K.R.T. Jones, T. Kapitula, and J. Powell. Nearly real fronts in a Ginzburg-Landau equation. *Proc. Roy. Soc. Edin. A*, **116**:193–206, 1990.

[15] C.K.R.T. Jones and N. Kopell. Tracking Invariant Manifolds with Differential Forms in Singularly Perturbed Systems. *Journal of Diff. Eq.* , **108**(1):64–88, 1994.

[16] T. Kapitula. Bifurcating bright and dark solitary waves of the nearly nonlinear cubic-quintic Schrödinger equation. *to appear in Proc. Roy. Soc Edin. A*, 1997.

[17] S.E. Newhouse. Lectures on Dynamical Systems. In *Dynamical Systems, C.I.M.E. Lectures Bressanoe, Italy June 1978, Progress in Math.* , volume **8**, pages 1–114. Birkhäuser-Boston: Boston, 1980.

[18] C. Robinson. Sustained resonance for a nonlinear system with slowly varying coefficients. *SIAM Math. An.* , **14**:847–860, 1983.

[19] C. Soto-Treviño and T.J. Kaper. Higher-order Melnikov theory for adiabatic systems. *J. Math. Phys.*, **37**:6220–49, 1996.

[20] W. van Saarloos and P. C. Hohenberg. Fronts, pulses, sources and sinks in generalized complex Ginzburg-Landau equations. *Physica D*, **56**:303–367, 1992.

[21] S. Wiggins. *Introduction to Applied Nonlinear Dynamical Systems and Chaos.* Springer Verlag New York etc., 1990.